SwRI-3943

# EVALUATION OF A HYDROGEN RESISTANT TITANIUM ALUMINIDE ALLOY

FINAL TECHNICAL REPORT
(Covering the Period September 90 - December 91)

by

**K. S. CHAN**

SOUTHWEST RESEARCH INSTITUTE
P. O. Drawer 28510
San Antonio, TX 78228-0510



Prepared for

THE TEXAS ENGINEERING EXPERIMENT STATION
College Station, Texas 77843
Subcontract No. 90-545

and

NATIONAL AERONAUTICS AND SPACE ADMINISTRATION
NASA-Ames Research Center
Moffett Field, California 94035
Contract No. NAG2-683


SOUTHWEST RESEARCH INSTITUTE

# TABLE OF CONTENTS

# LIST OF TABLES

# LIST OF FIGURES

## LIST OF FIGURES
(contintued)

# EVALUATION OF A HYDROGEN RESISTANT TITANIUM ALUMINIDE ALLOY

## ABSTRACT

The Ti-24Al-11Nb (Ti-24-11) alloy heat-treated to the fine basketweave microstructure was shown previously to be hydrogen-tolerant. In order to assess its limit of hydrogen tolerance, the tensile, creep, fracture toughness, and sustained load crack growth behaviors of this alloy were studied as a function of hydrogen content. All test specimens were thermally charged with internal hydrogen and tested at 25 and 600°C. Coupon specimens were used for developing the hydrogen-charging procedures and for studying compatibility of the alloy with high-temperature, high-pressure gaseous hydrogen. The mechanical test results indicated that the fine basketweave microstructure was tolerant to hydride embrittlement for hydrogen contents up to ≈1500 wt. ppm, providing that the hydride formed was of the $TiH_2$-type. On the other hand, hydrogen charging experiments indicated that the Ti-24-11 alloy was severely cracked and pulverized under zero load when the hydrogen content exceeded 3000 wt. ppm. X-ray diffraction results revealed that the dichotomous behaviors might be due to the formation of $TiH_{1.924}$-type hydrides at higher hydrogen contents. Thus, hydrogen embrittlement in the Ti-24-11 alloy with the fine basketweave microstructure depends on hydrogen content and the nature of hydrides formed.

# INTRODUCTION

Two of the materials that had been considered for possible applications in the National Aero-Space Plane (NASP) were the $Ti_3Al$- and TiAl-based intermetallic alloys. For these applications, the candidate materials will encounter high-temperature, high-pressure gaseous hydrogen [1,2]. Since hydrogen is known to cause embrittlement in many alloys and intermetallics, compatibility between material and high-temperature, high-pressure gaseous hydrogen must therefore be examined before either of the two titanium aluminide alloys can be used in the NASP.

Recent studies have shown that $Ti_3Al$-based alloys are susceptible to hydrogen embrittlement. In the second NASA Hydrogen Workshop [1], it was reported that $Ti_3Al$ was attacked by hydrogen [3]. Hydride formation was observed in both the Ti-24Al-11Nb and stoichiometric $Ti_3Al$ alloys charged with $H_2$ [3-6]. The hydrides were observed, via transmission electron microscopy, to lie on the prism planes in the Ti-24-11 alloy, and on the basal planes in the stoichiometric $Ti_3Al$ alloy. The fracture strength and ductility of $H_2$-charged Ti-24-11 were reduced in tension, but the yield strength increased under compression [7]. Zero ductility was observed in this alloy when the $H_2$ content reached 4000 wt. ppm [3]. In a 13.8 MPa gaseous $H_2$ environment, Ti-24-11 specimens subject to a constant stress of 75% of the ultimate tensile strength failed in 50 hours at 93°C, but failed in only 4 hours at 204°C [8]. The Ti-25Al-10Nb-3V-1Mo alloy (Super Alpha-Two) showed significant decreases in both elongation and reduction in area upon exposure to hydrogen [8,9]. The fracture mechanisms were predominantly cracking in the $\alpha_2$ phase and at the $\alpha_2/\beta$ interface. In contrast, fracture occurred in the $\beta$ phase when the alloy was tested in a He environment at the same pressure [10].

In the Third NASA Hydrogen Workshop [2], it was reported that two-phase TiAl-base alloys, [7,8] like $Ti_3Al$-alloys, were susceptible to hydrogen embrittlement in high-temperature, high-pressure gaseous hydrogen environments [11-14]. Based on this information, the use of either the $Ti_3Al$- or the TiAl-based alloys for NASP applications does not appear feasible.

In a recent study by Chan [15], the feasibility of developing hydrogen-tolerant microstructures for Ti-24Al-11Nb by heat-treatment processing was reported. A total of thirteen different microstructures was prepared, and their susceptibility to hydrogen embrittlement was screened using the Vickers hardness and tensile tests. One particular fine basketweave microstructure was found to tolerate the presence of up to 1300 wt. ppm internal hydrogen without exhibiting a loss of tensile ductility or stress rupture after 140 hours of creep at 95% of the yield stress (527 MPa). These results suggest that the fine basketweave microstructure is tolerant to hydrogen embrittlement for the test conditions and hydrogen contents investigated. However, the range of temperatures and hydrogen contents at which the hydrogen-tolerant behavior prevails has not been investigated, nor the effects of hydrogen on other mechanical properties such as fracture toughness, elevated-temperature creep, and sustained-load crack growth studied.

In a different study, Majumdar et al. [16] found that Ti-25Al-10Al-3V-1Mo exhibited extensive cracking and pulverization when exposed to high-temperature (510°C), high-pressure (13.6 MPa) hydrogen. On the other hand, neither cracking nor pulverization was observed in the Ti-24Al-11Nb alloy when it was exposed to 13.6 MPa hydrogen pressure at 538°C for 100 hours [15]. This difference in behaviors is not well understood and has not been studied.

The objective of this program was to evaluate the range of temperatures, properties, and hydrogen contents within which the fine basketweave microstructure is resistant to hydrogen embrittlement. The scope of work in this program was divided into four tasks: (1) evaluation of the tensile behavior; (2) evaluation of fracture toughness; (3) evaluation of creep behavior; and (4) evaluation of sustained-load crack growth behavior. Property evaluations for all four tasks were performed at 25 and 600°C and at hydrogen contents up to 2750 ppm. by weight. Thermal annealing in high-temperature, high-pressure gaseous hydrogen was selected as the means for introducing

hydrogen into the test specimens. By varying the hydrogen charging conditions, the effects of high-temperature, high-pressure hydrogen on cracking and pulverization in the Ti-24Al-11Nb alloy with the fine basketweave microstructure were studied.

## EXPERIMENTAL PROCEDURES

### A. Material

The Ti-24Al-11Nb titanium aluminide alloy was obtained from TIMET of Henderson, NV, in the form of a 12.7 mm-thick hot-rolled plate. The ingot alloy was forged at 1150°C, followed by a β anneal at 1178°C. It was then hot rolled at 982°C to 1038°C, with a final anneal at 982°C for 15 minutes, and then air cooled. The alloy compositions in weight percent were 13.5 pct Al, 21.3 pct Nb, 0.039 pct Fe, 0.58 pct $O_2$, 0.003 pct $N_2$, and balance Ti. Eight pieces of Ti-24-11 blocks 31.8 mm in width, 61.3 mm in length, and 12.7 mm in thickness were heat-treated to obtain the fine basketweave microstructure using the procedures developed earlier [15]. The heat-treatment procedures included (1) solutionizing at 1100°C in argon for one hour, followed by fan cool to room temperature, and (2) aging at 815°C in argon for 8 hours and then fan-cooled to ambient temperature. The fine-basketweave microstructure, shown in Figure 1, was identical to that obtained in previous investigations [15,17].

### B. Specimen Geometry

After heat-treatment, the blocks were machined into tensile, creep, single-edge-notched (SEN), and compact-tension (CT) specimens. Design and dimensions of the tensile and creep specimens were identical, as shown in Figure 2(a). A total of 16 tensile and creep specimens were prepared. Two SEN specimens were machined initially but one was lost during fatigue-precracking.

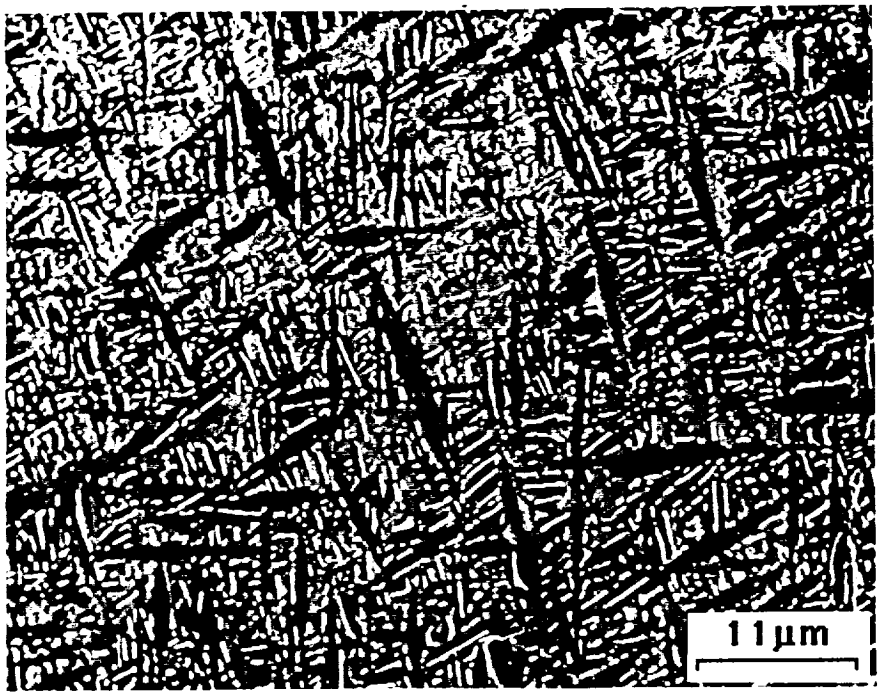


(a)

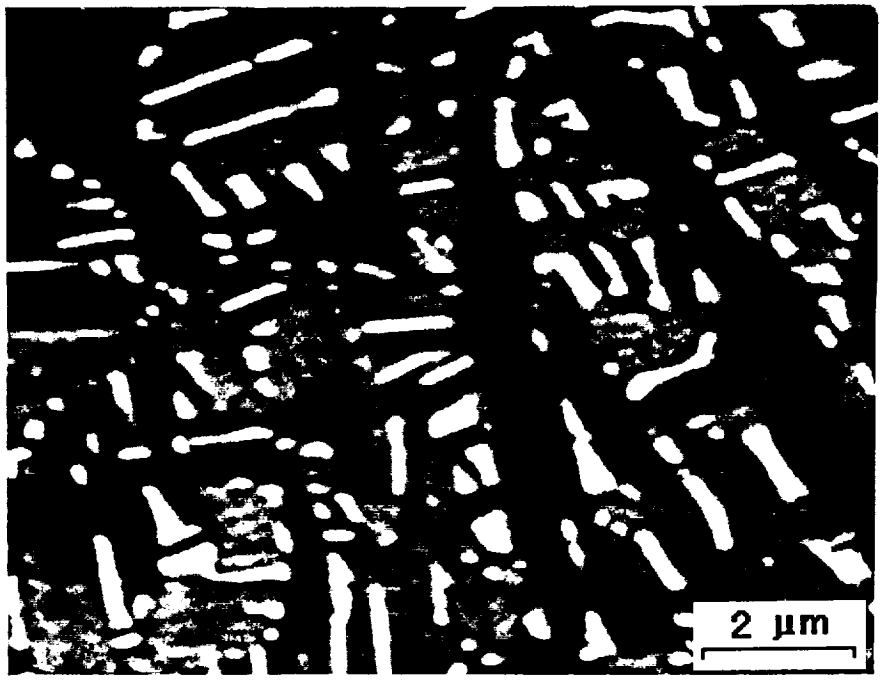


(b)

Figure 1. SEM micrographs of Ti-24Al-11Nb with the fine basketweave microstructure showing the $\alpha_2$ matrix (dark phase) and the discontinuous β phase (light phase).

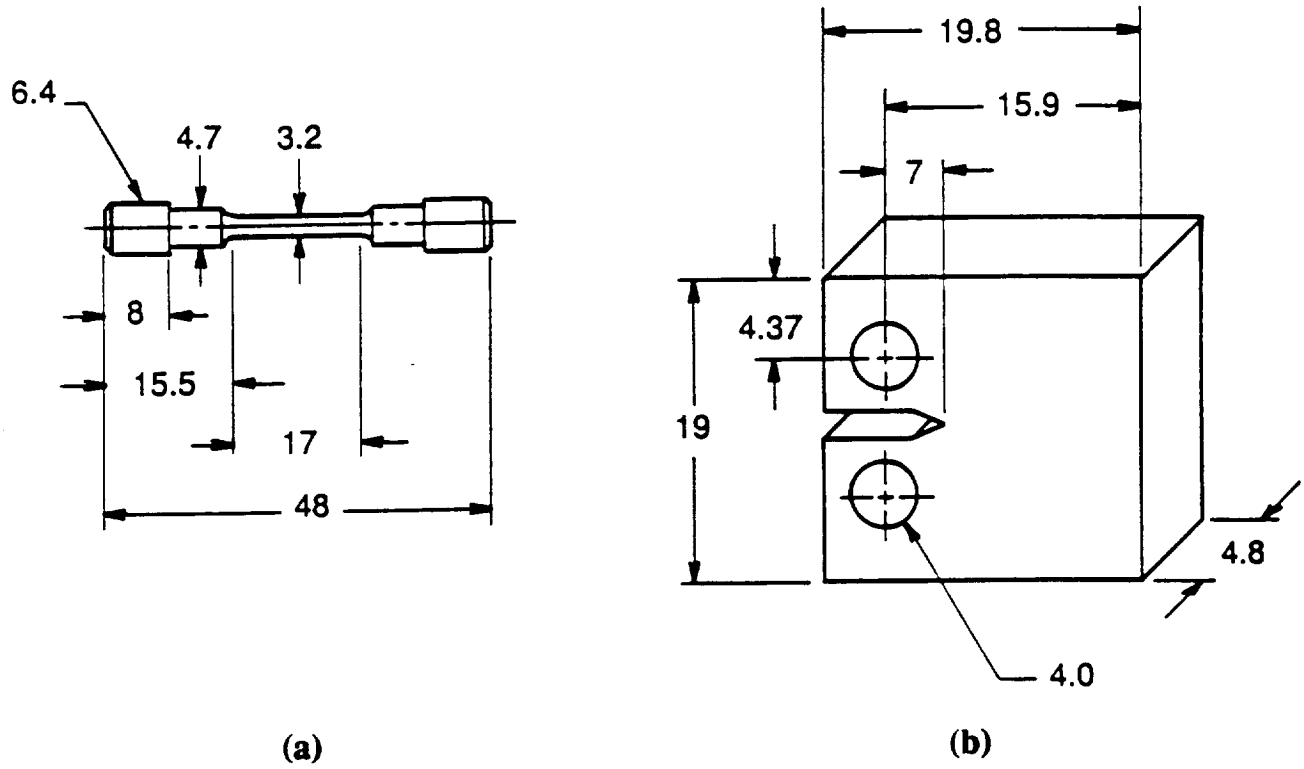


Figure 2. Dimensions of tensile and creep specimens (a), and compact-tension specimens (b) used in this study.

In the interest of reducing machining and specimen size, four compact-tension specimens, whose dimensions are shown in Figure 2(b), were machined as replacements for the lost SEN specimen. The CT specimens were used for fracture toughness and sustained load crack growth tests. Furthermore, coupon specimens about 10 mm x 10 mm x 12.7 mm were used for developing the hydrogen-charging procedures.

## C. Hydrogen Charging Procedures

Hydrogen charging was performed in (1) a large autoclave, (2) a hydrogen stress rupture apparatus, and (3) a small autoclave. Different hydrogen pressures, charging temperatures, and heating rates were explored in developing the procedures for obtaining 5000 wt. ppm in the fine basketweave microstructure. The initial hydrogen-charging efforts were based on thermal anneals of the coupon specimens at hydrogen pressures in the range of 6.8 to 20.4 MPa gaseous hydrogen at 538°C. These severe charging conditions generally, though not always, led to severe cracking and pulverization of the coupon specimens. A summary of the hydrogen charging results is presented in Table I. After many trials, the small autoclave was selected for performing all of the hydrogen charging operations. Designed and built for this program, the small autoclave consisted of a furnace and a 31.8 mm diameter 304 stainless pipe with caps and tubing connected to a hydrogen source. During hydrogen charging, the specimens were placed at the center of the autoclave in a basket made out of stainless steel screen. Both temperature and pressure were monitored continuously during the charging operation.

The process developed for introducing hydrogen into the test specimens was a two-step procedures that involved (1) a thermal anneal at 732°C in 0.1 MPa helium for 30 minutes, and (2) a thermal anneal at 538°C for 16 hours in a gas mixture containing 0.1 MPa helium and various hydrogen partial pressures ranging from 0.1 MPa to 13.8 MPa. By varying the hydrogen pressure, it was possible to obtain intact specimens containing 150 to 2750 wt. ppm internal hydrogen, as

well as severely cracked and pulverized specimens whose hydrogen contents were in excess of 10,000 wt. ppm. In all cases, the heating rate was maintained at 193°C/hour. These procedures were used for charging hydrogen into tensile, creep, and fracture specimens.

Hydrogen contents of individual coupon specimens were initially analyzed by National Spectrographic Laboratories (NSL) in Cleveland, Ohio, where the measurements were performed using a Leco Hydrogen Analyzer. The maximum hydrogen content that could be determined via this technique was 5000 wt. ppm, which was short of the anticipated hydrogen concentration in many charged specimens. As a result, many of the coupon specimens and all of the tensile, creep, and fracture specimens were sent to Luvak, Inc., in Boylston, MA, for hydrogen content determination. The techniques employed at Luvak were (1) vacuum hot extraction for hydrogen contents less than 12,700 wt. ppm, and (2) vacuum fusion for hydrogen contents greater than 19,000 wt. ppm.

## D. Mechanical Testing

After hydrogen charging, all of the test specimens were electropolished prior to testing. Tensile, creep, fracture toughness, and sustained load crack growth tests were performed according to the test matrix shown in Table II. Tensile tests were conducted at 25 and 600°C at a strain rate of $5 \times 10^{-6}$ $sec^{-1}$ using a servo-hydraulic testing machine equipped with an induction heat unit. The same setup was used for creep tests, which were performed at 25 and 600°C. The constant load creep tests at 25°C were conducted at 527 MPa; none of the specimens failed prior to the discontinuation of tests after 140-160 hours of creep. A constant initial stress of 300 MPa was used for creep tests at 600°C, which were run until the specimens ruptured.

Fracture toughness tests were performed at 25 and 600°C inside a scanning electron microscope (SEM) equipped with a high-temperature loading stage whose maximum temperature

capacity was 800°C [18]. During testing, the crack-tip region was photographed as a function of the stress intensity levels. The amount of crack extension at each stress intensity level was measured from the near-tip micrographs and used to obtain the K-resistance curve. The same experimental setup was also used for performing sustained load crack growth experiments at 600°C. A constant load was first applied to the cracked specimen. The near-tip region was then photographed as a function of time of load applied, usually at 30-minute intervals. The crack increment was measured from the SEM micrographs and divided by the time increment to obtain the sustained load crack growth rate. After several crack growth measurements were obtained at a given K level, the stress level was increased to interrogate the crack growth response at a higher K level.

After testing, almost all of the test specimens were sent to Luvak for hydrogen content determination. In addition, X-ray diffraction was performed at 25°C on selected specimens to investigate whether or not hydrides were present in these specimens. In all cases, X-ray diffraction was performed at 40 KV using $CuK_{\alpha}$ radiation with a Ni filter. The X-ray peaks were then identified by comparing with the standards established by JCPDS [19].

## RESULTS

### A. Tensile Behavior

The tensile results obtained in this study are summarized in Table III together with those reported earlier by Chan [15]. The results presented in Table III include the yield stress, ultimate tensile strength, total and plastic elongations, and hydrogen content for specimens tested at 25 and 600°C. In general, the present results are in agreement with the previous study [15]. The main difference between these two studies is in the tensile behavior of as heat-treated materials, Table III. In the previous study, the total elongation for the as heat-treated materials was 3%, while it was

≈8.5% in the present case (specimen 43). The higher elongation observed in specimen 43 was due to the activation of extensive twinning, which was absent in previous specimens and in other specimens in the present investigation.

A summary of the stress-strain curves for 25°C is presented in Figure 3 without including specimen 43. Figure 3 shows that the tensile results for 25°C are in agreement with the previous study [15], which indicated that the fine basketweave microstructure was tolerant to hydrogen under tensile straining at a strain rate of $5 \times 10^{-6}$ $sec^{-1}$ for hydrogen contents of up to 1300 wt. ppm. The present study showed that the limit of tolerance exhibited by the fine basketweave microstructure was as high as 1500 wt. ppm hydrogen, as a total elongation of approximately 3% was maintained at this hydrogen level. The dependence of plastic elongation on hydrogen content is presented in Figure 4. The results indicated that a plastic elongation of 1 to 2% was maintained by the fine basketweave microstructure at hydrogen contents up to 1500 wt. ppm, compared to zero ductility for an equiaxed microstructure and a coarse basketweave microstructure at $H_2$ content of ≈500 wt. ppm [15]. There was considerable scatter in the test data in Figure 4; the lowest value of plastic elongation observed was ≈1%, while 2.2% was the highest value observed in the charged specimens.

The stress-strain curves for 600°C are shown in Figure 5 for hydrogen contents of 640 and 1518 wt ppm hydrogen. For these hydrogen levels, hydrogen did not appear to affect appreciably the ultimate tensile strength or the total elongation. Compared to the ambient temperature behavior, the yield strength is lower and the total elongation is higher at 600°C at an equivalent hydrogen level.

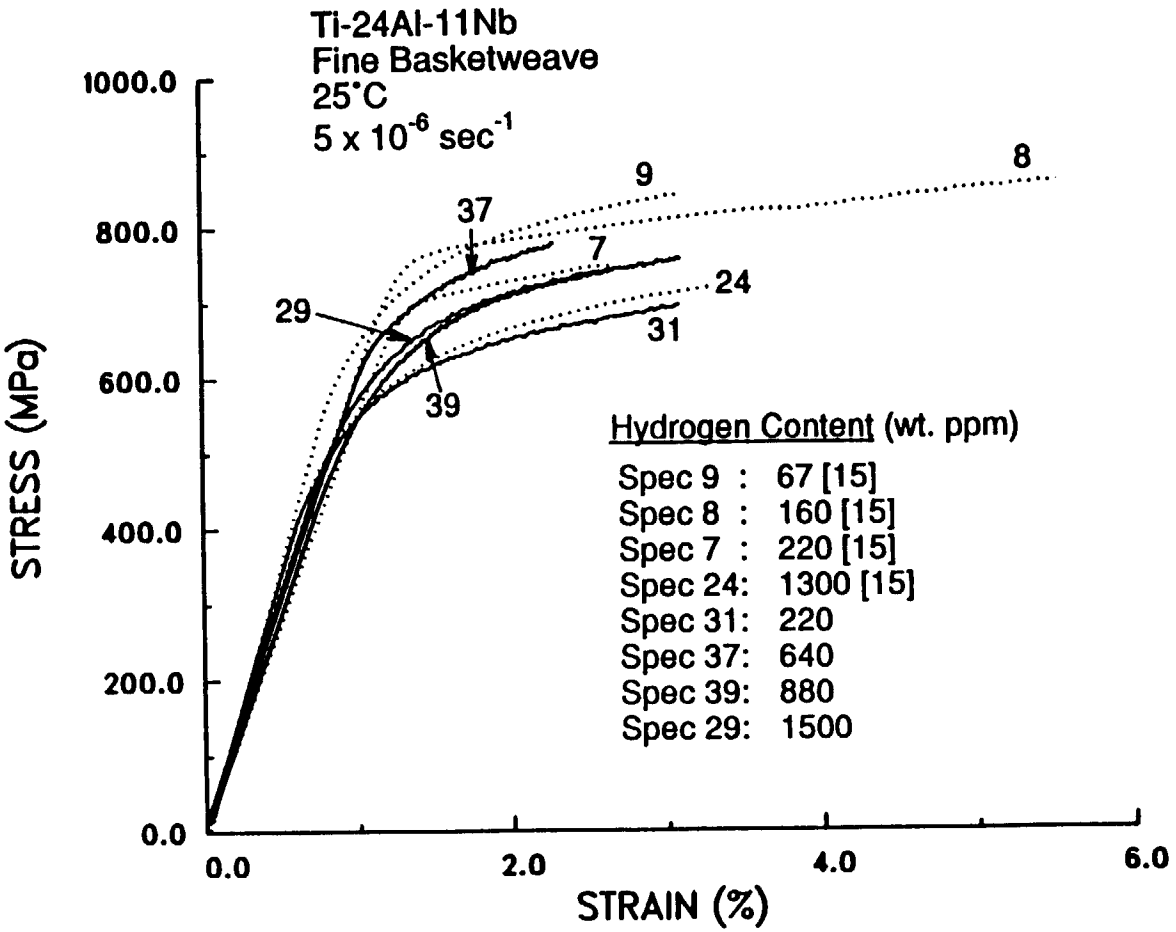


Figure 3. Engineering stress-strain curves of Ti-24Al-11Nb at 25°C and various hydrogen contents.

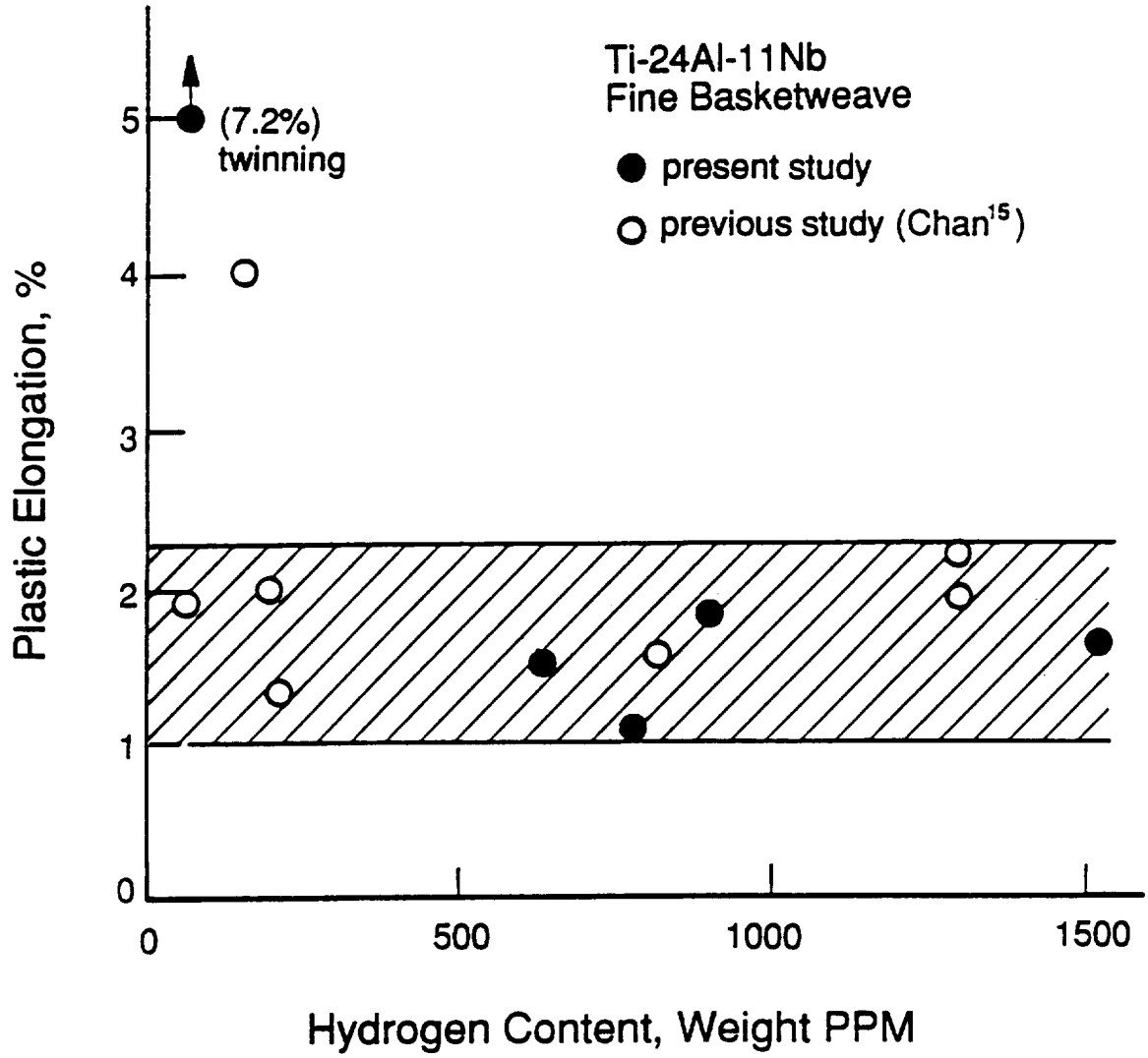


Figure 4. Plastic elongation of Ti-24Al-11Nb as a function of hydrogen content.

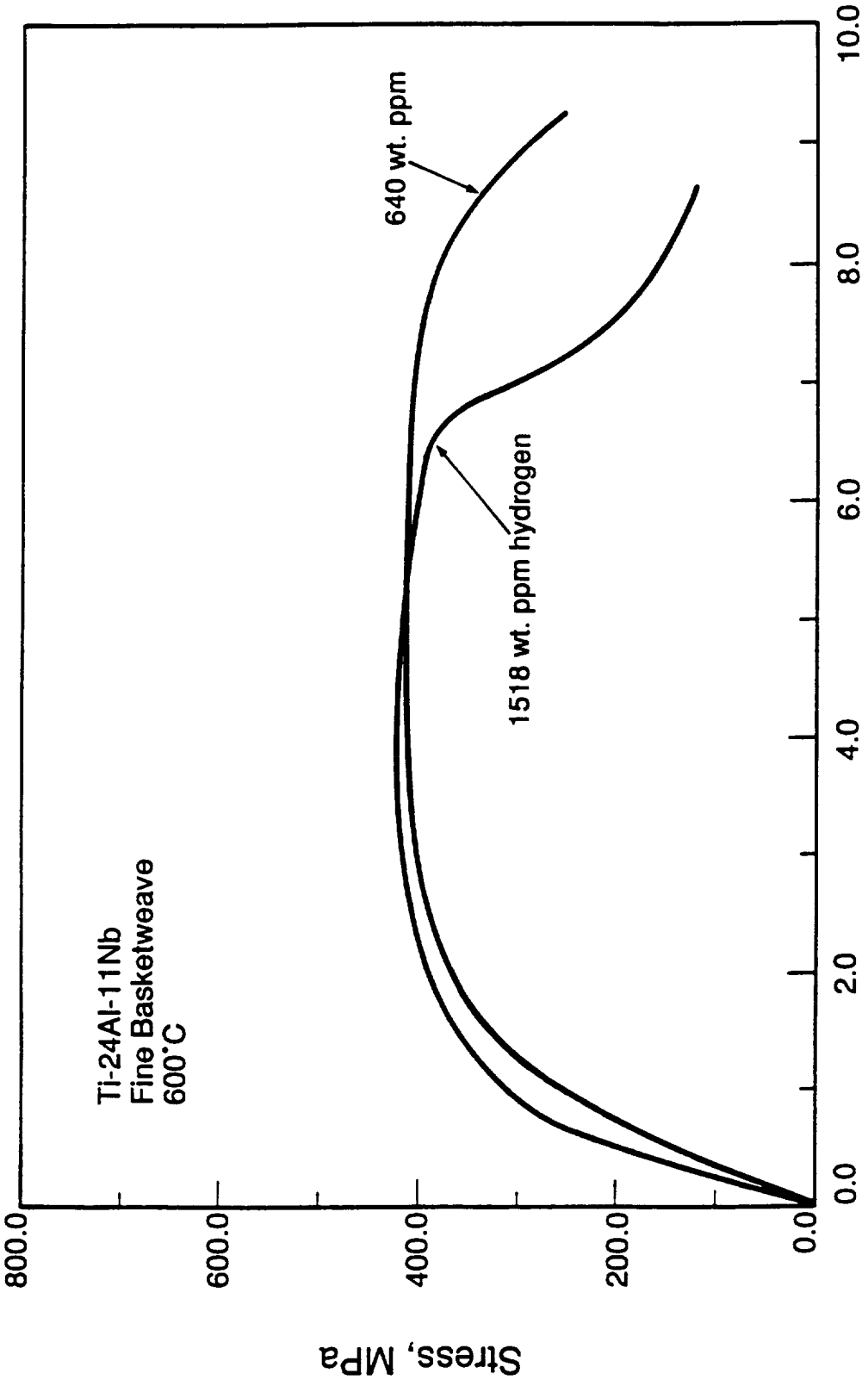


Figure 5. Engineering stress-strain curves of Ti-24Al-11Nb at 600°C and two hydrogen levels.

## B. Fracture Toughness

The ambient-temperature fracture toughness results of the Ti-24Al-11Nb are presented as K-resistance curves in Figure 6 for three hydrogen contents. In accord with the tensile ductility, the fracture toughness value decreased only slightly with increasing hydrogen contents. At a hydrogen content as high as 2750 wt. ppm hydrogen (specimen 317), the fine basketweave microstructure still maintained a toughness value of 12.5 MPa$\sqrt{m}$, compared to 14 MPa$\sqrt{m}$ for 156 wt. ppm $H_2$ and 15 MPa$\sqrt{m}$ for 39 wt ppm $H_2$ in the as heat-treated condition.

The fracture processes in the hydrogen-charged specimens at 25°C are presented in Figures 7 and 8 for hydrogen contents of 156 and 2750 wt. ppm, respectively. In both figures, the near-tip regions are shown as a function of the applied stress intensity, K, levels. At 156 wt. ppm hydrogen, fracture occurred by the formation of a localized zone of microcracks ahead of the main crack tip. The microcracks linked with the main crack upon increasing K levels and caused final failure at K = 14 MPa$\sqrt{m}$. This fracture process was essentially similar to that for the as heat-treated condition (39 wt. ppm hydrogen), whose failure process was reported earlier [17].

The near-tip region of specimen 317 (2750 wt. ppm hydrogen) was found to contain a fair number of microcracks after hydrogen-charging. These microcracks opened up upon increasing K levels from 2.5 to 9.0 and then to 11.0 MPa$\sqrt{m}$, as illustrated in Figure 8. Additional microcracks were also induced during the process. At K= 12.4 MPa$\sqrt{m}$, the microcracks linked together and coalesced with the main crack, leading to final fracture at K = 12.5 MPa$\sqrt{m}$.

The K-resistance curves for 600°C are shown in Figure 9. Increasing the hydrogen content reduced the stress intensity level at which the crack started to extend from $K_{IC}$ = 15 at 70 wt. ppm $H_2$ to $K_{IC}$ = 9 MPa$\sqrt{m}$ at 420 wt. ppm $H_2$. On the other hand, the crack growth resistance was increased once crack extension occurred. The amount of crack growth toughness increased with increasing hydrogen content, as evidenced by a higher slope in the K-resistance curve for 420 wt.

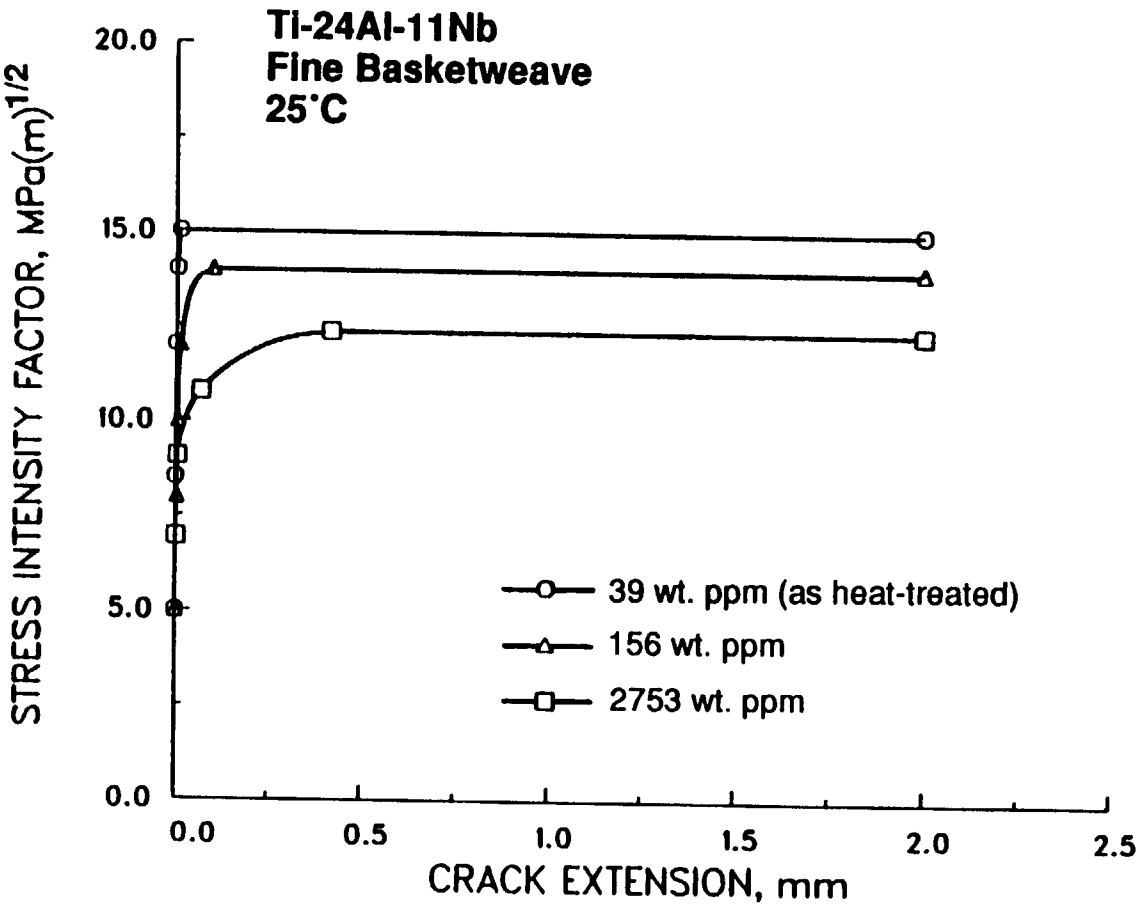


Figure 6. K-resistance curves of Ti-24Al-11Nb at 25°C and three hydrogen levels.

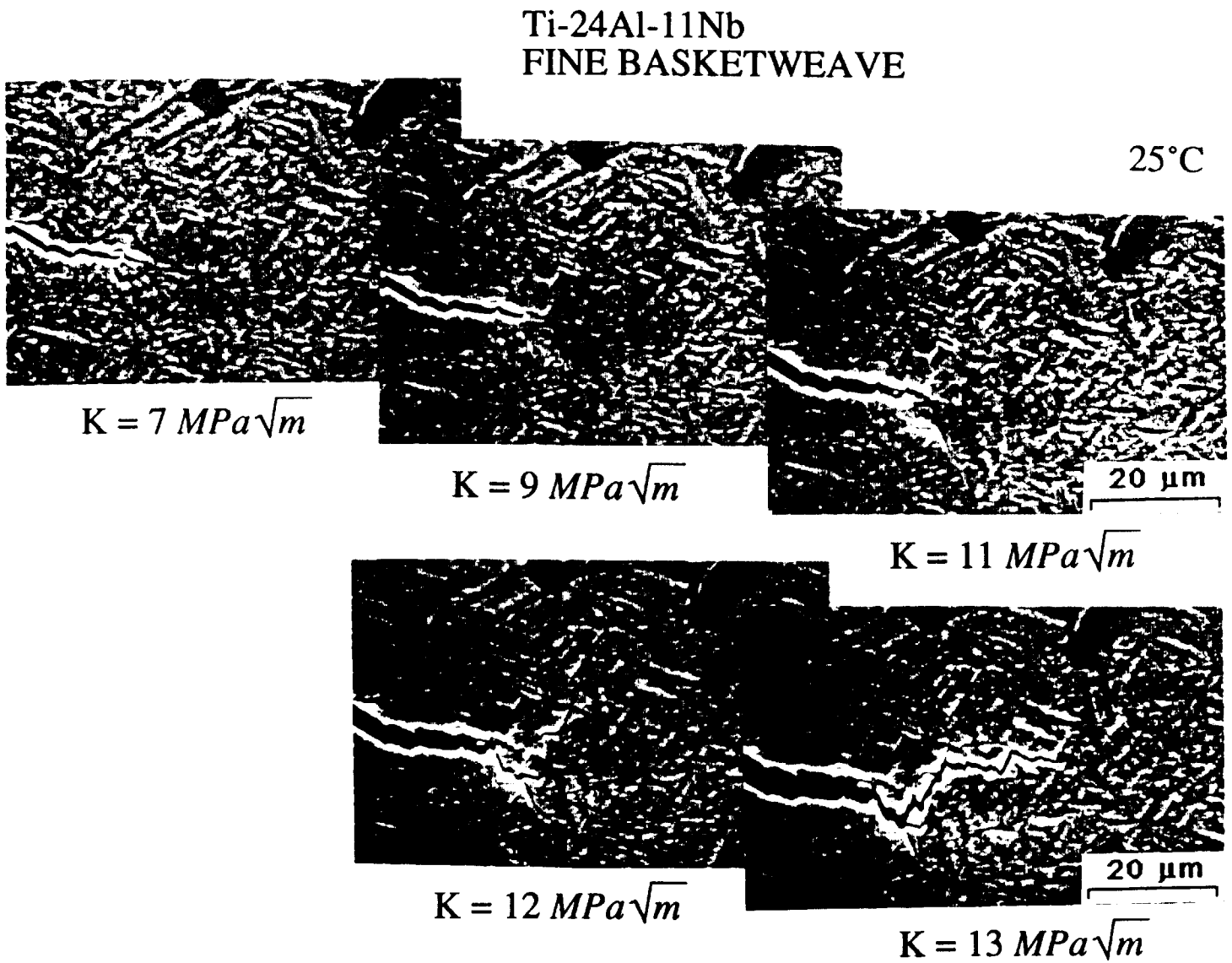


Figure 7. Near-tip fracture process in Ti-24Al-11Nb at 25°C under increasing K levels (hydrogen content = 156 wt. ppm).

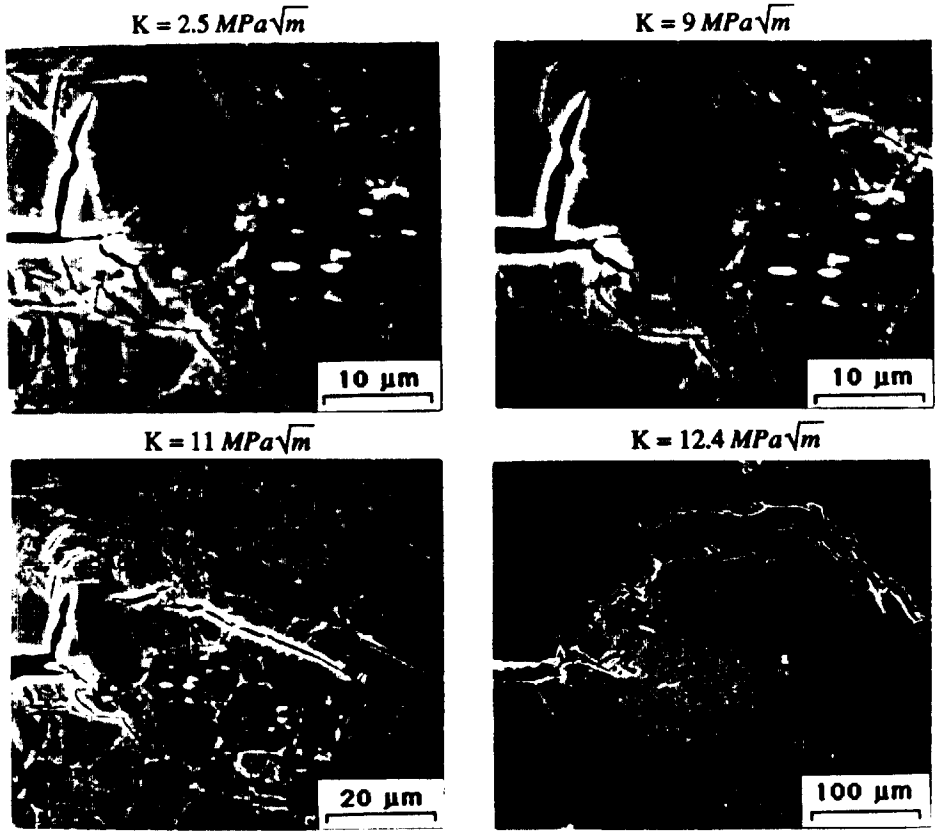


Figure 8. Opening of H-charging induced microcracks and their growth under increasing K levels in Ti-24Al-11Nb with 2750 wt. ppm hydrogen at 25°C.

ppm (Figure 9). In both H-charged and uncharged materials, extensive crack-tip blunting and microcracking occurred with increasing K levels and crack extensions. The fracture process observed at various K levels in the H-charged material with 420 wt. ppm hydrogen is shown in Figure 10, while that for the uncharged material is similar and has been reported elsewhere [17].

## C. Creep and Stress Rupture Behavior

Creep tests at 25°C were performed at an initial constant stress of 527 MPa. The creep curves for three hydrogen levels are shown in Figure 11. The creep strain exhibited by the fine basketweave microstructure increased slightly with increasing hydrogen content. None of the creep specimens tested at 25°C failed after 140-160 hours of creep. Tensile tests of post-creep specimens at 25°C revealed total elongations in the range of 1.5 to 2.0%.

Creep tests at 600°C were conducted at an initial constant stress of 300 MPa. Mixed effects of hydrogen on the creep rupture life were observed at this temperature, Figure 12. In the range of 80 to 1045 wt. ppm hydrogen, the creep rupture life was essentially unaffected by hydrogen; the rupture life, however, was reduced for the specimen charged with ≈1300 wt. ppm hydrogen.

## D. Sustained-Load Crack Growth Behavior

The crack growth mechanisms in the uncharged specimen under a sustained load at 600°C are summarized in Figure 13 for K levels of 5 and 22 MPa$\sqrt{m}$. At K = 5 MPa $\sqrt{m}$, the initial crack growth process involved the nucleation of a microcrack ahead of the main crack after the load was applied for ≈0.5 hr, Figure 13(a). The microcrack increased in length with increasing time of loading, Figure 13(b), and eventually linked with the main crack. Subsequent crack growth occurred

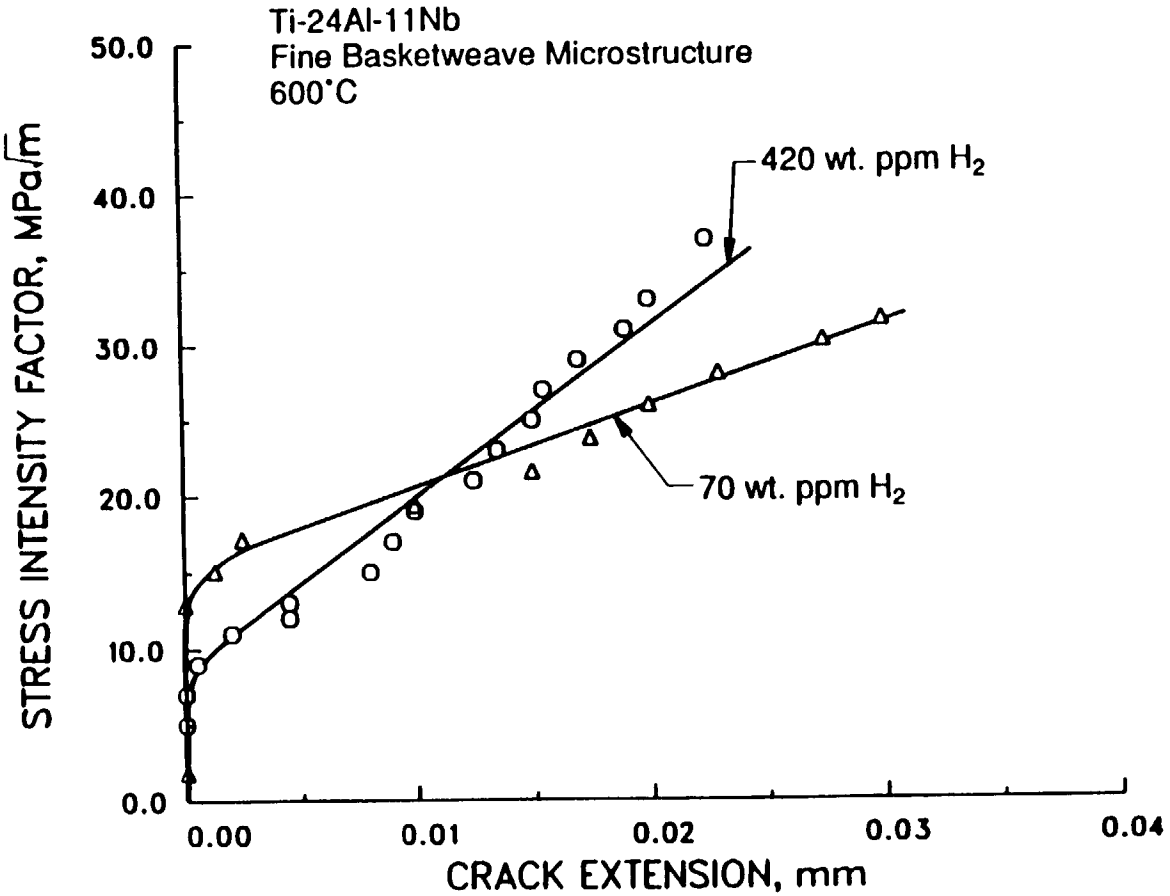


Figure 9. K-resistance curves of Ti-24Al-11Nb at 600°C for hydrogen contents of 70 and 420 wt. ppm.

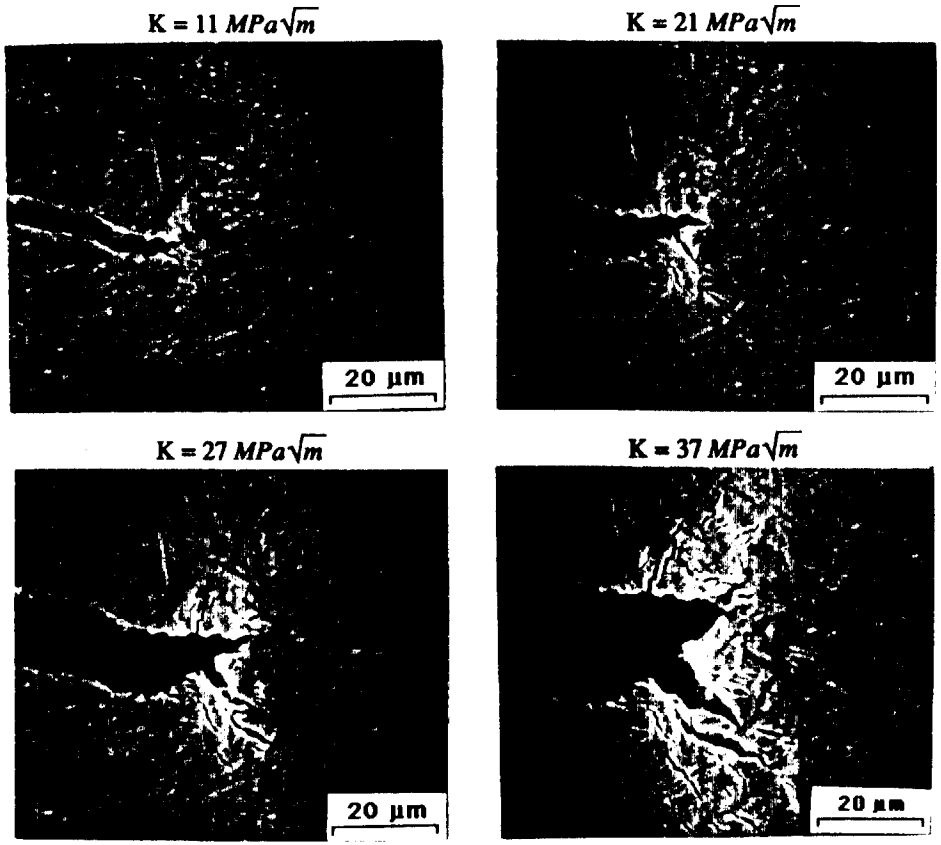


Figure 10. Crack-tip blunting and microcracking in Ti-24Al-11Nb under increasing K levels for 600°C (hydrogen content = 420 wt. ppm).

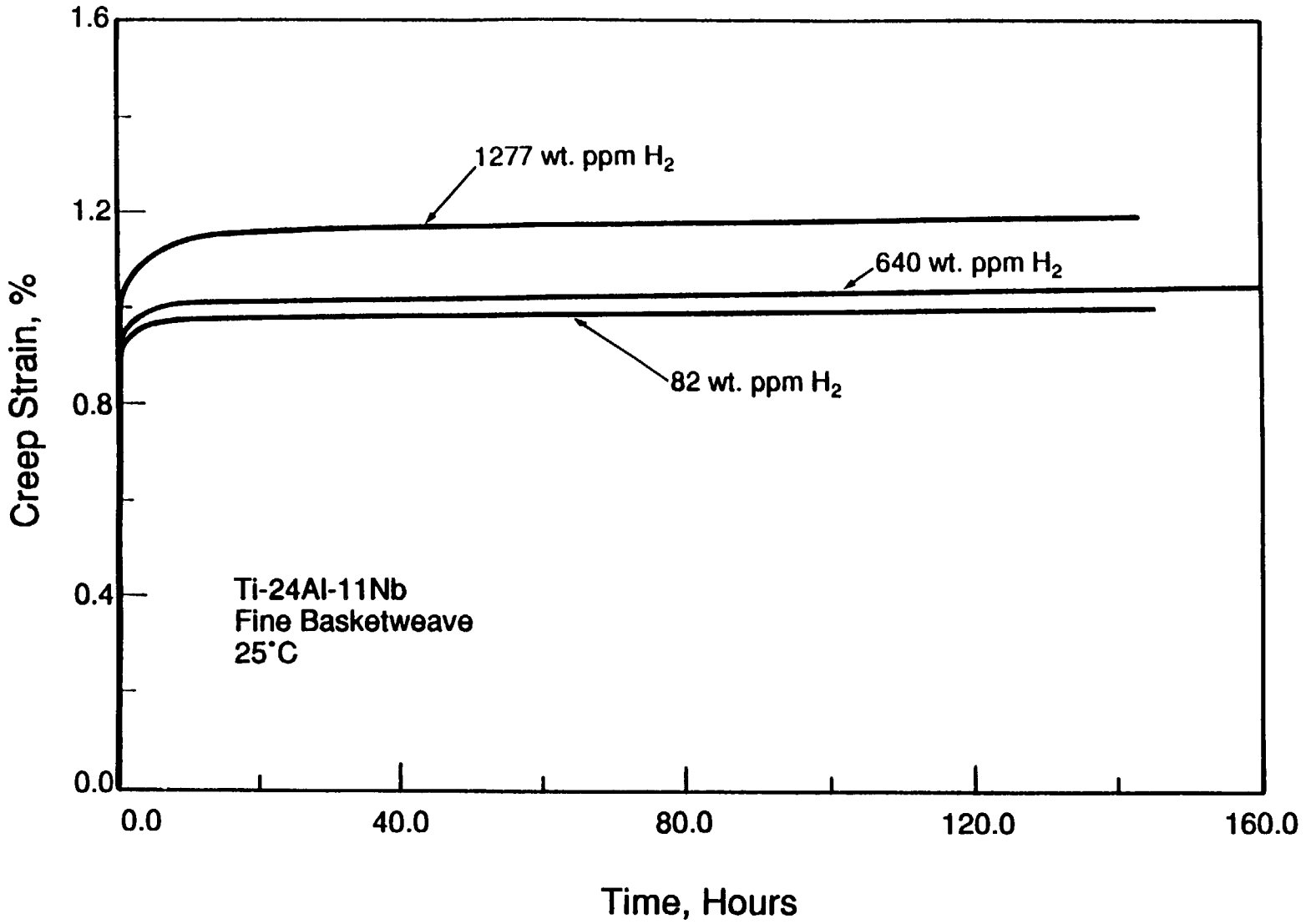


Figure 11. Creep curves of Ti-24Al-11Nb at 527 MPa for 25°C showing increasing creep strain with increasing hydrogen contents.

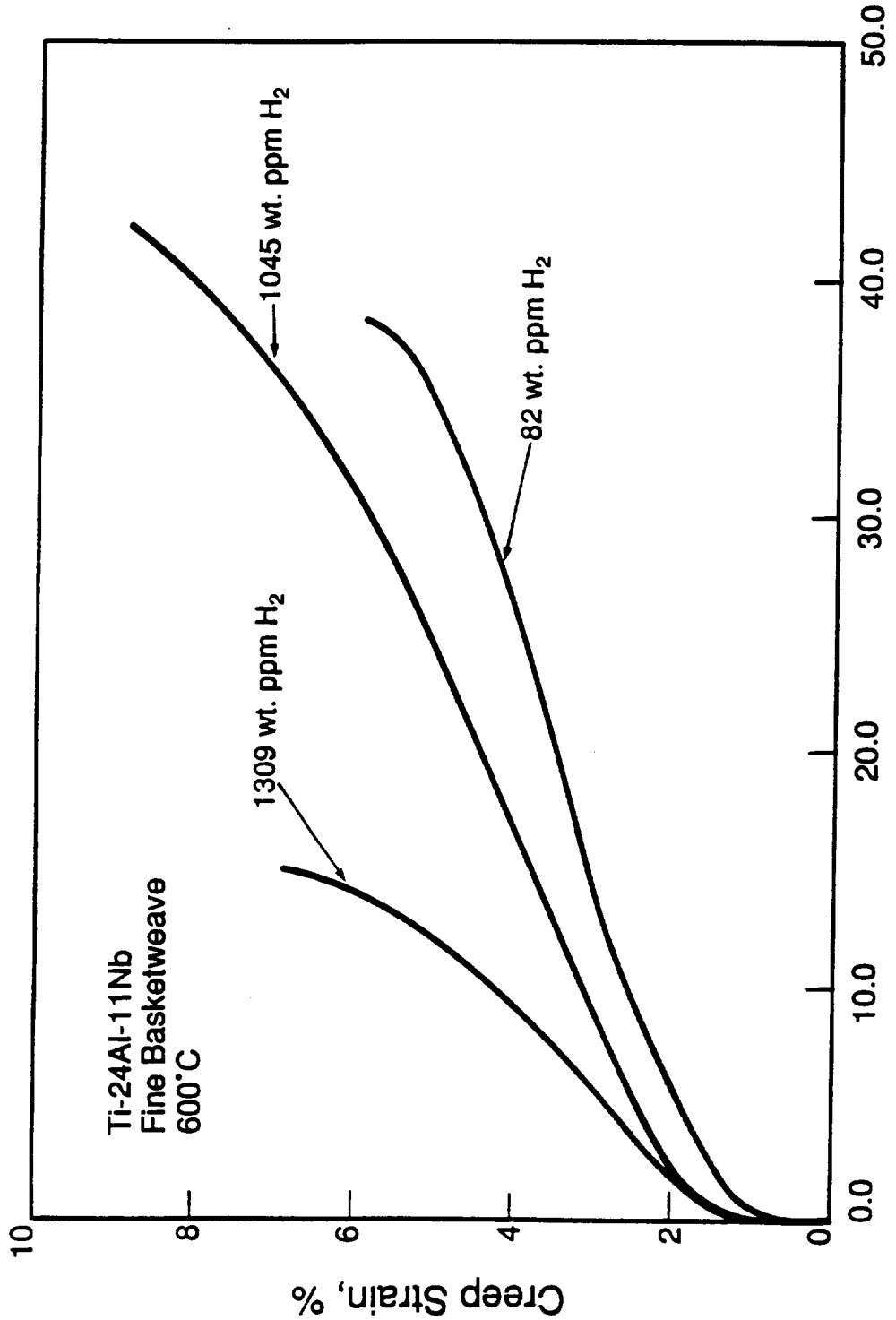


Figure 12. Creep curves of Ti-24Al-11Nb at 300 MPa for 600°C showing a reduction in rupture life at 1300 wt. ppm hydrogen.

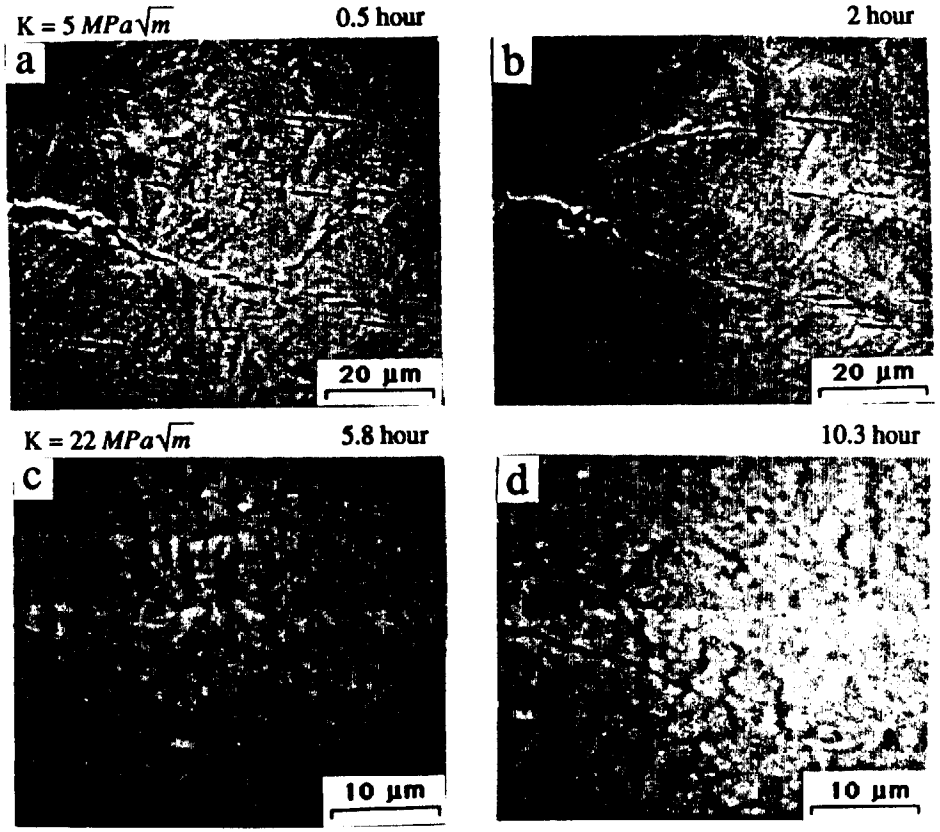


Figure 13. Sustained load crack growth mechanisms in uncharged Ti-24Al-11Nb (70 wt. ppm hydrogen) at 600°C under K levels of 5 and 22 MPa$\sqrt{m}$.

by direct extension of the main crack without microcrack nucleation, growth, and coalescence occurring ahead of the crack tip, which remained sharp throughout the K range (5 to 26 MPa$\sqrt{m}$) examined, Figures 13(c) and (d).

The crack growth mechanisms in the H-charged specimen at sustained K levels of 5 and 10 MPa$\sqrt{m}$ are shown in Figure 14. As in the uncharged condition, crack growth in the hydrogen-charged specimen occurred by a direct crack extension process without microcrack formation ahead of the main crack tip, Figures 14(a) and (b). The direct crack growth process continued at K levels of 8 and 10 MPa$\sqrt{m}$. At these K levels, the main crack developed bifurcated tips but the growth process appeared to be dominated by a single branch of the crack tip, as illustrated in Figures 14(c) and (d). The test specimen failed at K > 10 MPa$\sqrt{m}$ due to a machine malfunction. As a result, no crack growth data were obtained for K > 10 MPa$\sqrt{m}$.

The sustained load crack growth rates for the H-charged and uncharged materials are compared in Figure 15. Each data point in Figure 15 represents averages of three to eight crack growth rate measurements at a given K level. The result indicates that within the small range of H contents studied, the sustained load crack growth rate is not affected by hydrogen.

## E. Pulverization Behavior

The Ti-24Al-11Nb alloy cracked and pulverized at high hydrogen contents. Both cracking and pulverization occurred during hydrogen charging at relatively high hydrogen pressures. A summary of the charging results is presented in Figure 16 in terms of hydrogen content, hydrogen pressure, and specimen condition after hydrogenation. As indicated earlier, the charging conditions were a half-hour anneal at 732°C in 0.1 MPa helium, followed by a 16-hour anneal at 538°C in a gaseous environment containing 0.1 MPa helium and a hydrogen pressure that varied from 0.1 Mpa to 13.8 MPa. These hydrogen charging conditions resulted in intact specimens with 136 to 2750 wt.

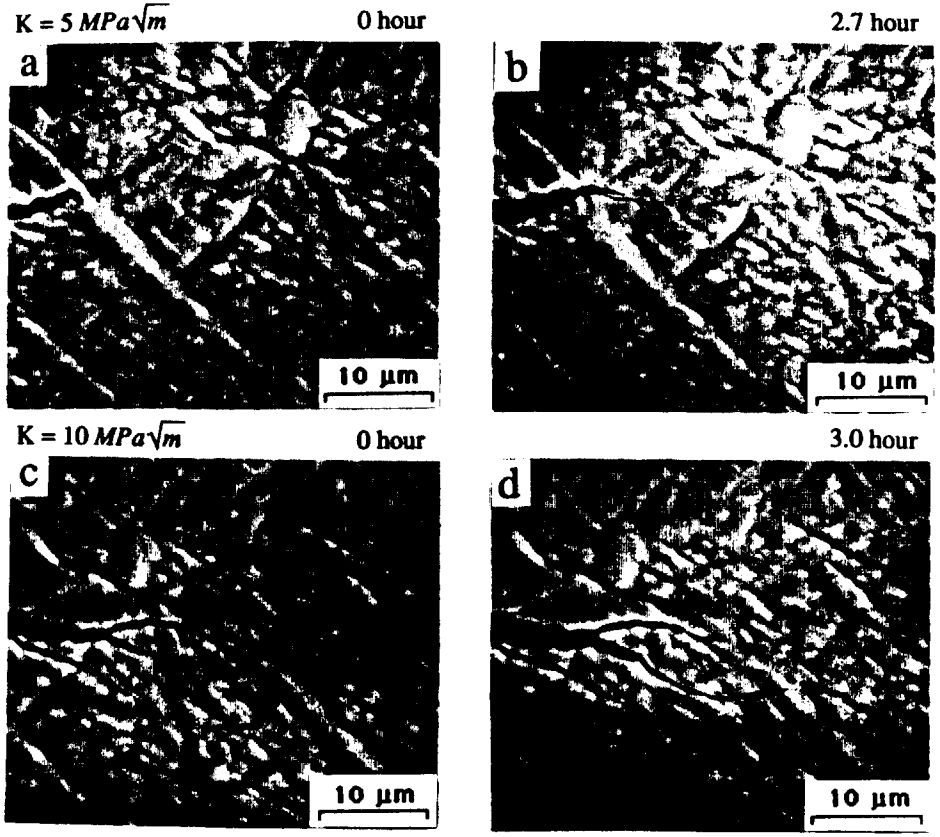


Figure 14. Sustained load crack growth mechanisms in H-charged Ti-24Al-11Nb (134 wt. ppm hydrogen) at 600°C under K levels of 5 and 10 MPa$\sqrt{m}$.

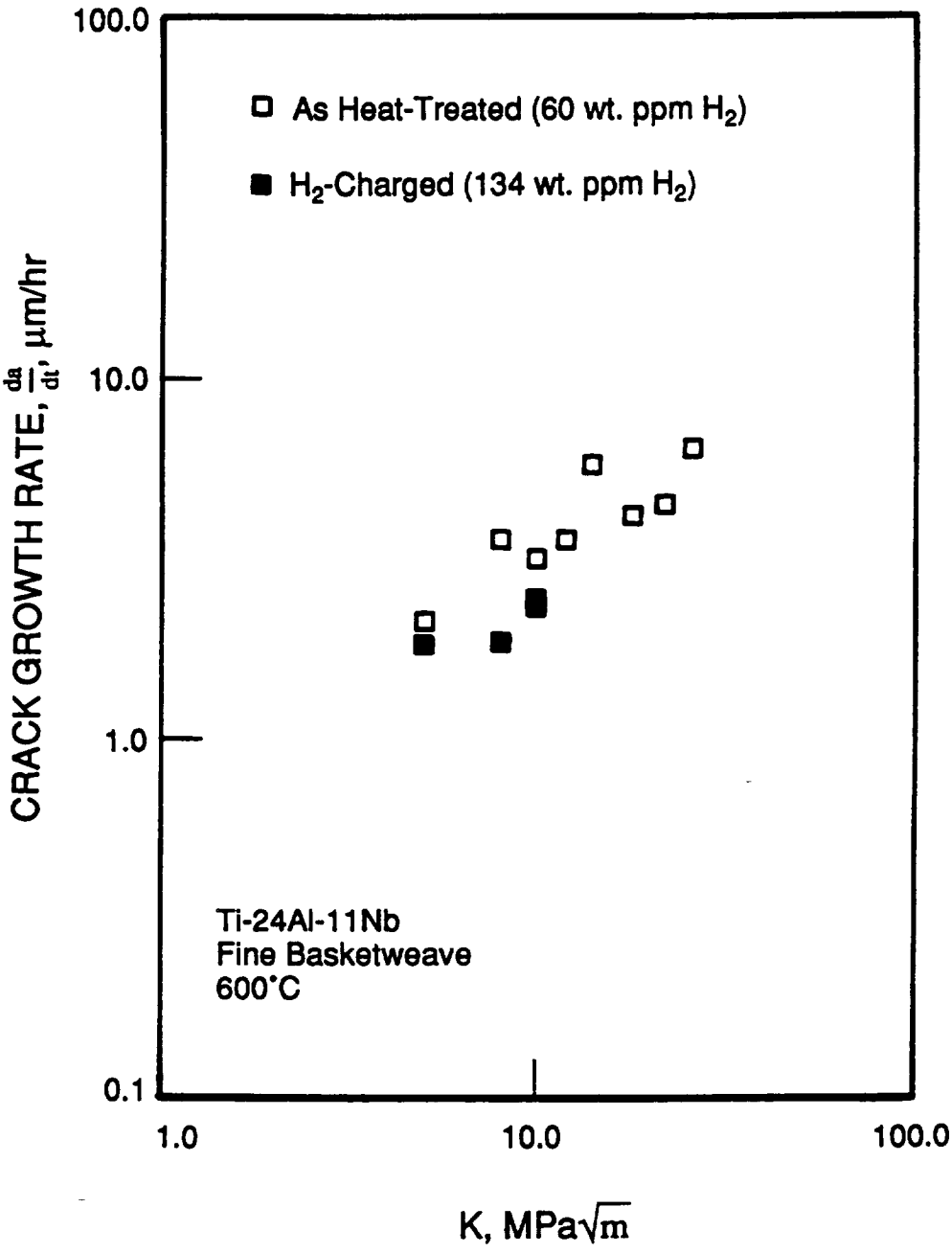


Figure 15. Sustained load crack growth results for uncharged (70 wt. ppm hydrogen) and charged (134 wt. ppm hydrogen) Ti-24Al-11Nb showing the absence of hydrogen embrittlement.

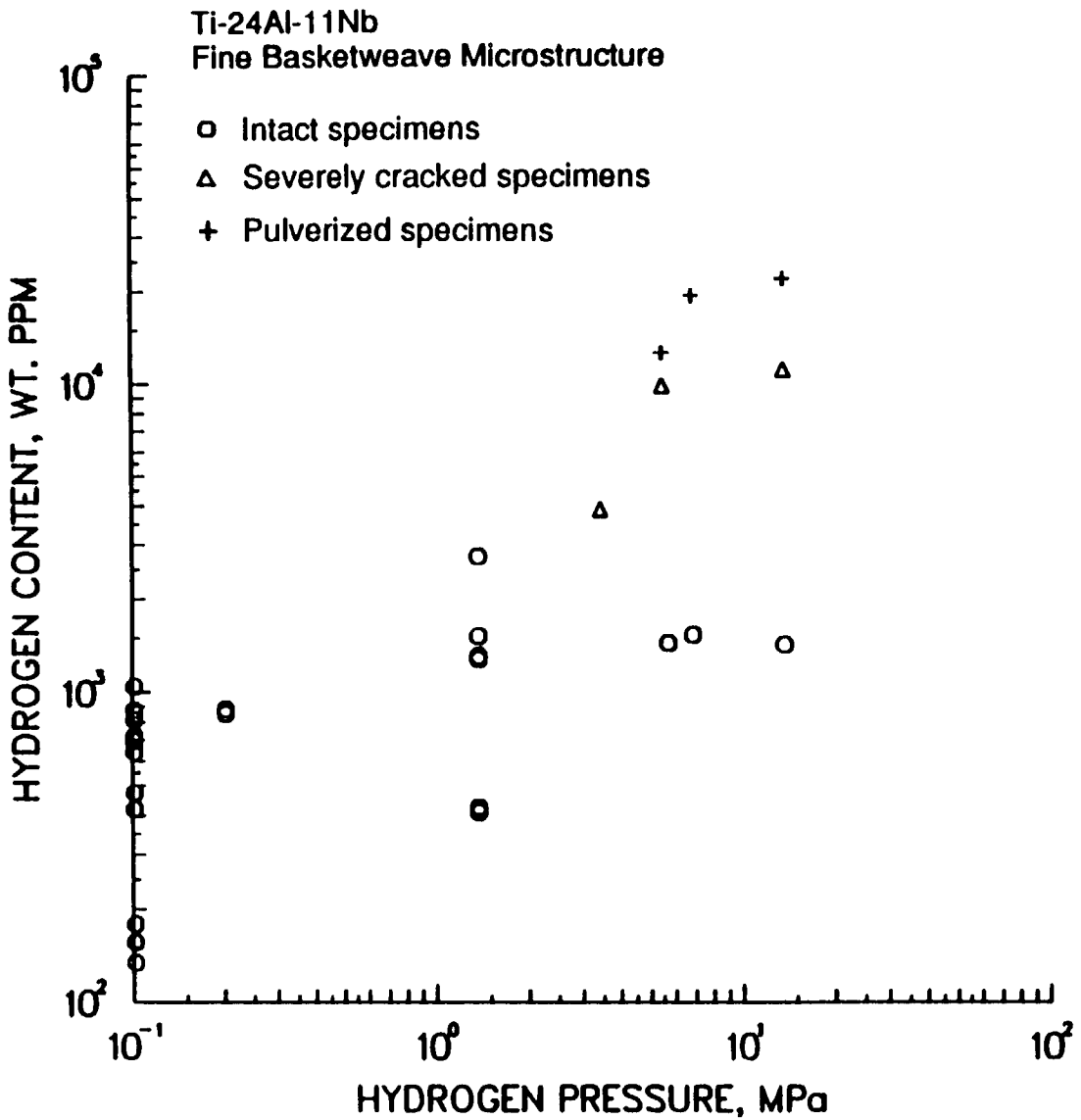


Figure 16. Hydrogen contents of Ti-24Al-11Nb after thermal charging at 538°C in gaseous hydrogen at various pressures.

ppm hydrogen when the hydrogen pressure was between 0.1 and 1.36 MPa. Charging at a hydrogen pressure of 3.4 MPa or above led to cracking and pulverization of the specimens. Figure 17(a) shows a tensile specimen that exhibited extensive cracking and broke into many pieces after charging to contain 9880 wt. ppm hydrogen at 3.4 MPa hydrogen pressure, while the crack pattern observed in a coupon specimen charged to 3910 wt. ppm is shown in Figure 17(b). The coupon specimens were pulverized into particles ranging from 1-5 mm in diameter when charged to exceed 10,000 wt. ppm hydrogen.

Charging at a high hydrogen pressure (e.g., 6.8 MPa) did not always lead to cracking or pulverization of the Ti-24-11 alloy, Figure 16. Examining the surface of the intact specimens by Auger spectroscopy revealed the presence of a thin oxygen-rich surface layer approximately 2400 μm in thickness, Figure 18. In contrast, similar oxygen-rich surface layers were not present in either the cracked or semi-pulverized specimens. A summary of the Auger spectroscopy results is presented in Table IV. The oxygen-rich layers were observed in specimens that did not receive a short time anneal at 732°C and were exposed to a gaseous hydrogen environment for a relatively long duration (e.g., 100 hours). The result suggests that the oxygen-rich surface layer might have acted as a kinetic barrier that reduces the intake of hydrogen into the test specimens during hydrogen charging. The existence of such a kinetic barrier helps explain the relatively large variation in the hydrogen contents of the test specimens despite receiving identical charging conditions.

To better understand the cracking and pulverization behaviors, X-ray diffraction (XRD) was performed on the intact, cracked, and pulverized specimens to determine whether hydrides were present in the specimens. Summarized in Table V, the XRD results suggest the presence of two types of hydrides, which were identified as $TiH_2$ and $TiH_{1.924}$ in the Ti-24-11 alloy with the fine basketweave microstructure. Note that many forms of titanium hydrides are possible in titanium aluminides. Ternary hydrides in the form of $(Ti_3Al)H_x$ have been reported by Rudman, et al. [20]. Additional forms of hydrides whose identities are yet to be determined have also been observed in

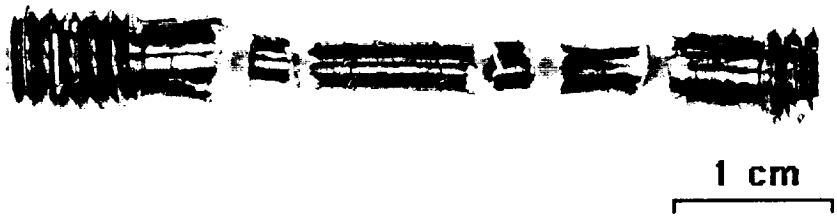


(a)

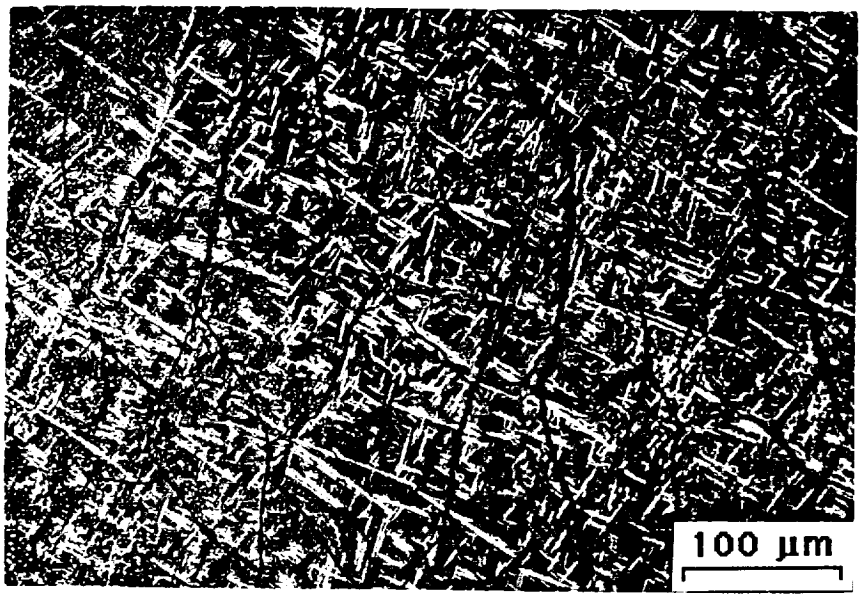


(b)

Figure 17. Crack patterns in Ti-24Al-11Nb: (a) tensile specimen charged with 9880 wt. ppm hydrogen, and (b) coupon specimen charged with 3910 wt. ppm hydrogen.

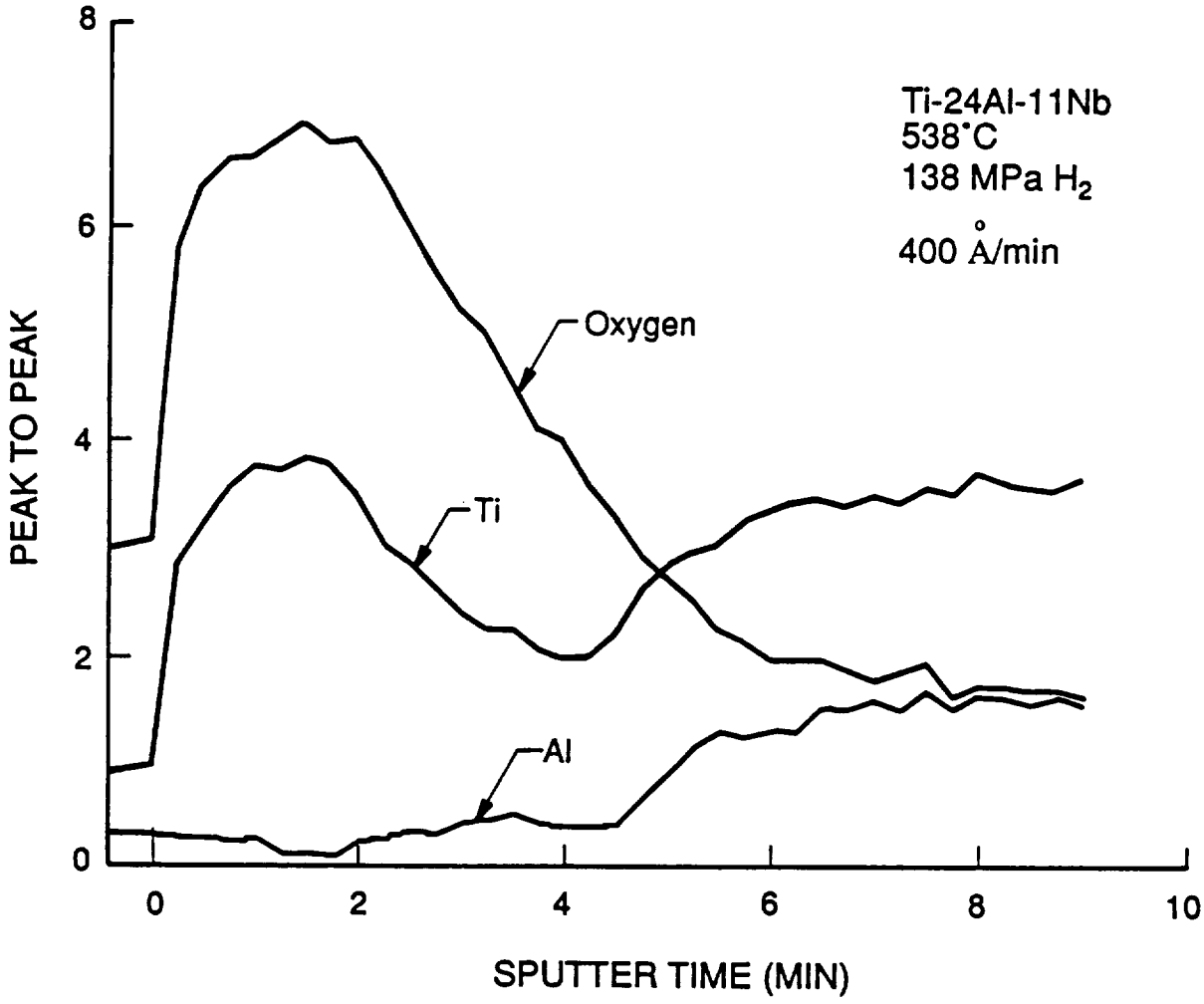


Figure 18. Auger Electron Spectroscopy (AES) depth profile obtained for a Ti-24Al-11Nb specimen which remained intact after charging for 100 hours in 13.8 MPa hydrogen at 538°C.

$Ti_3Al$ and TiAl-alloys [4,21,22]. XRD standards for these hydride phases are not available. Attempts to match the observed XRD patterns with TiH [23,24], $TiH_{0.71}$, NbH, and a beta-Ti alloy [25] all led to negative results. Based on the information currently available, the observed XRD patterns matched those for $TiH_2$ [26] and $TiH_{1.924}$ [26,27] the best. It is possible that these hydrides contain ternary elements. For this reason, they will be referred to $TiH_2$- and $TiH_{1.924}$-type hydrides. Basically, four different X-ray diffraction patterns were observed in these specimens. The uncharged specimen (specimen 328, 70 wt. ppm hydrogen) exhibited a XRD pattern corresponding to $Ti_3Al$, Figure 19(a). Specimens that remained intact after hydrogen charging and contained 147 to ≈1500 wt. ppm hydrogen showed a XRD pattern that included peaks of $Ti_3Al$ and $TiH_2$, Figure 19(b). The angular (2θ) positions of most of the strongest peaks for $TiH_2$ and $Ti_3Al$ occurred at close proximity (less than a fraction of one deg). The strongest evidence for the presence of $TiH_2$ was the (211) peak of $TiH_2$, which occurred at ≈71.0 deg in Figure 19(b), but is absent in the pattern for $Ti_3Al$ in Figure 19(a). When the hydrogen content was 1400 to 2750 wt. ppm, diffraction peaks for the $TiH_{1.924}$ hydride appeared in the XRD pattern, resulting in a XRD pattern containing $Ti_3Al$, $TiH_2$, and $TiH_{1.924}$ peaks. The strongest evidence for the presence of $TiH_{1.924}$ is the (311) peak of the $TiH_{1.924}$, which occurred at 70° in Figures 19(c) and 19(d), but in neither Figure 19(a) nor Figure 19(b). At hydrogen contents in excess of 10,000 wt. ppm, all of the specimens were pulverized and their XRD patterns appeared to be the sum of $TiH_2$ and $TiH_{1.924}$, with little evidence for the presence of $Ti_3Al$ in the pulverized specimens, Figure 19(e).

## DISCUSSIONS

The results of this investigation reveal that hydrogen affects the mechanical properties of Ti-24Al-11Nb with the fine basketweave microstructure in two distinctly different manners depending on the hydrogen content. At hydrogen contents less than 1500 wt. ppm, hydrogen appears to have little or minor effect on the tensile ductility, fracture toughness, creep rupture, and sustained

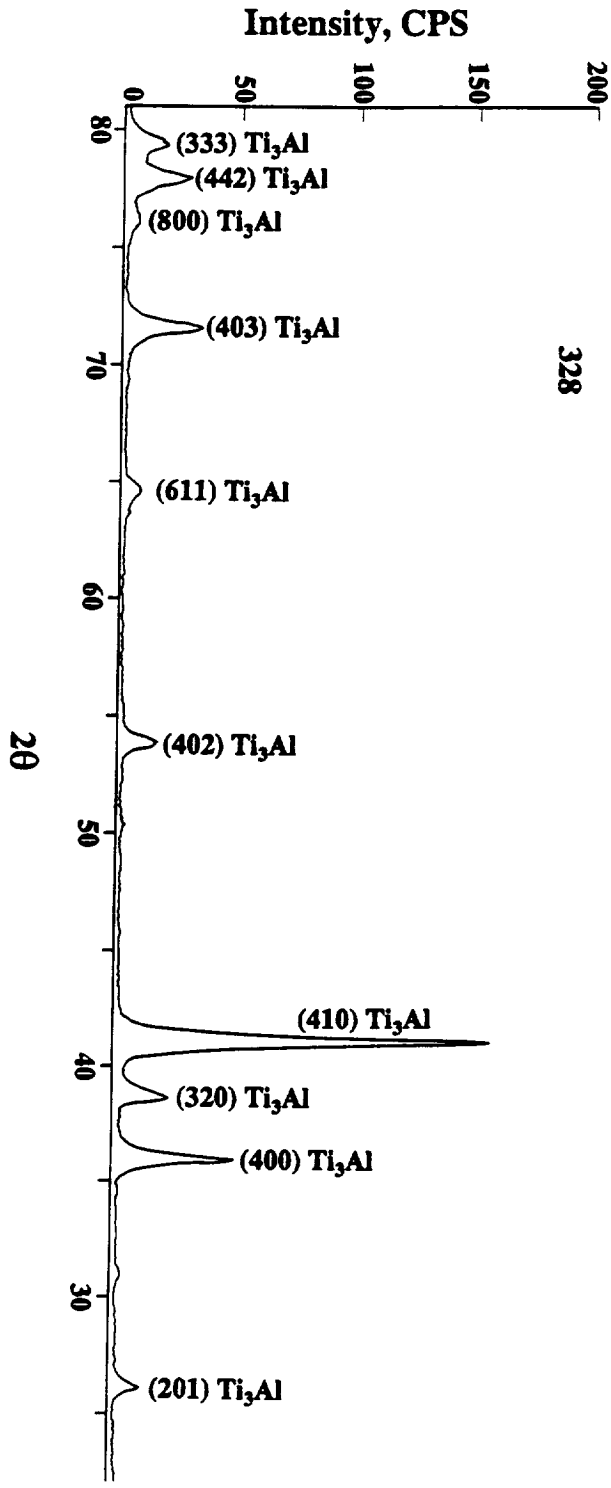


(a)

Figure 19. XRD patterns for Ti-24Al-11Nb: (a) $Ti_3Al$ pattern observed in specimen 328 (70 wt. ppm hydrogen).

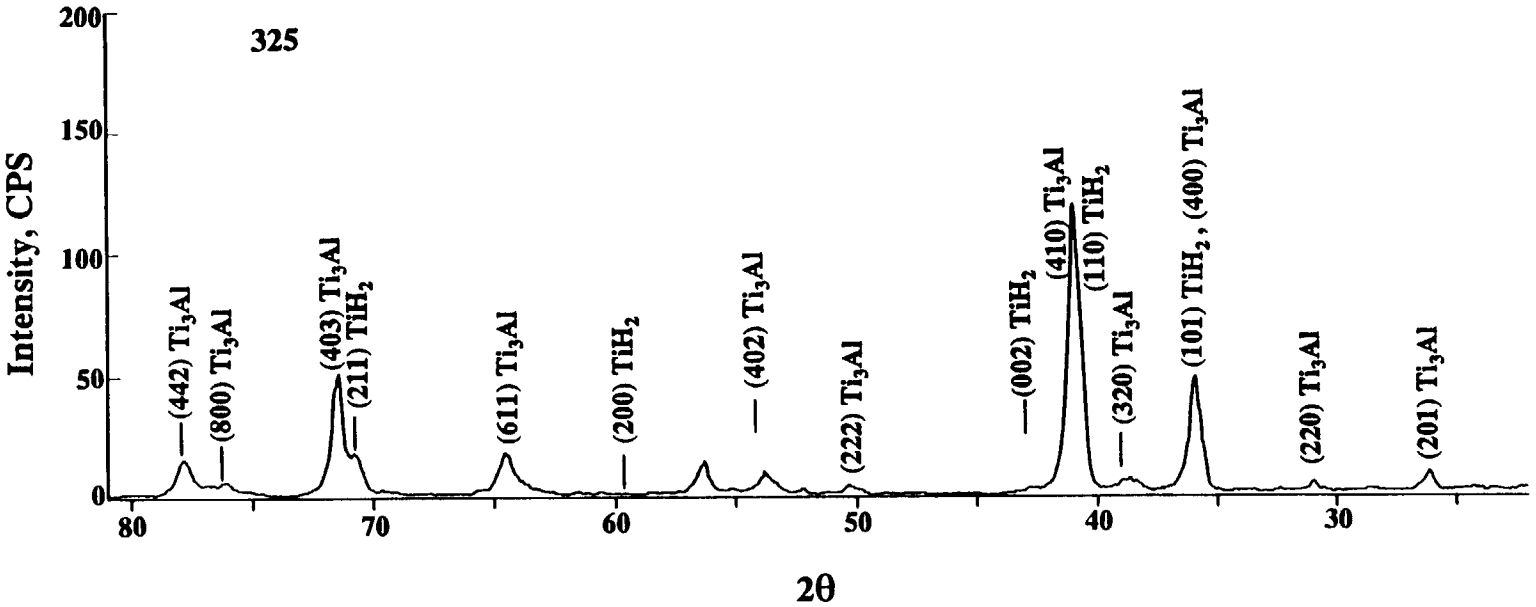


(b)

Figure 19. (cont'd) XRD patterns for Ti-24Al-11Nb: (b) $Ti_3Al$ plus $TiH_2$ patterns observed in specimen 325 (156 wt. ppm hydrogen).

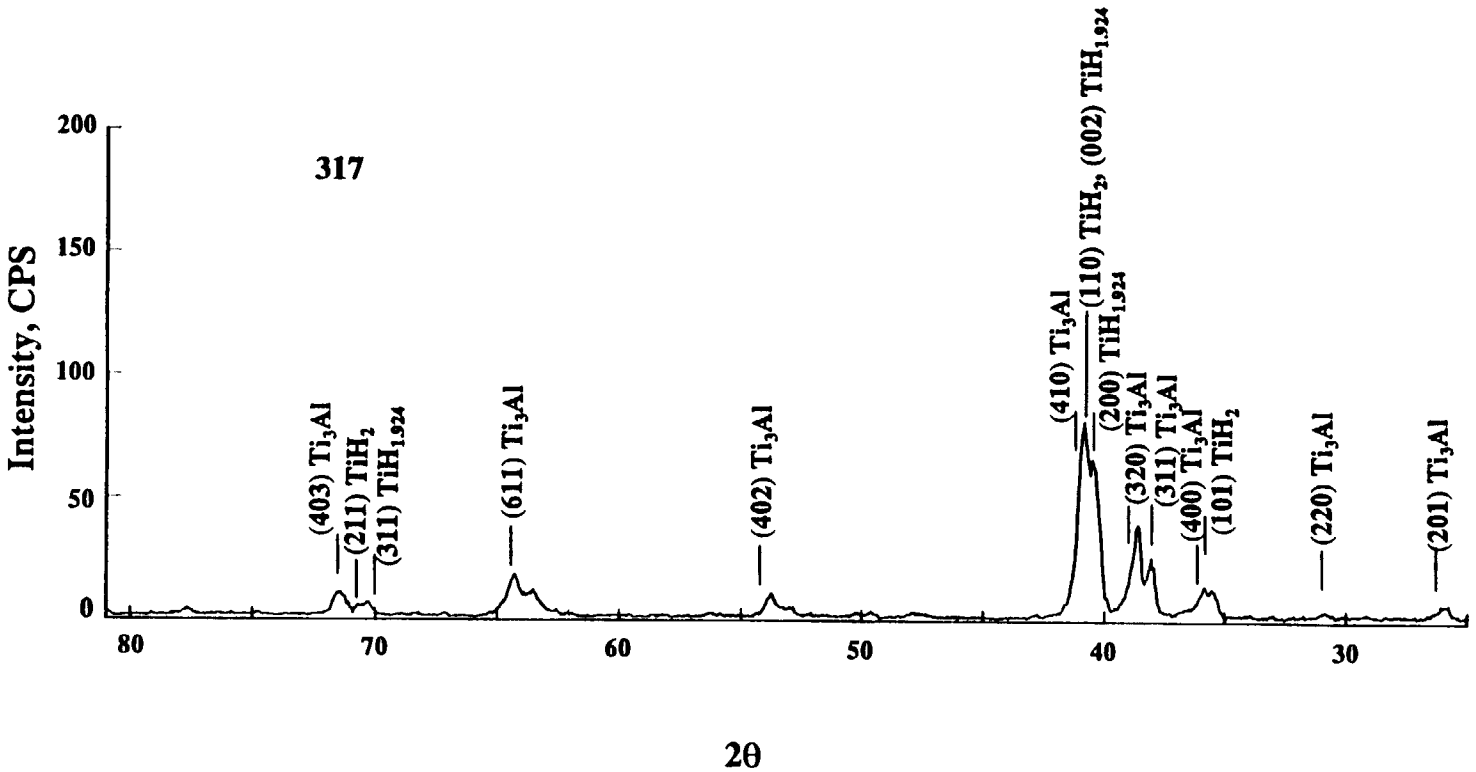


(c)

Figure 19. (cont'd) XRD patterns for Ti-24Al-11Nb: (c) $Ti_3Al$, $TiH_2$, and $TiH_{1.924}$ patterns observed in specimen 29 (1520 wt. ppm hydrogen).

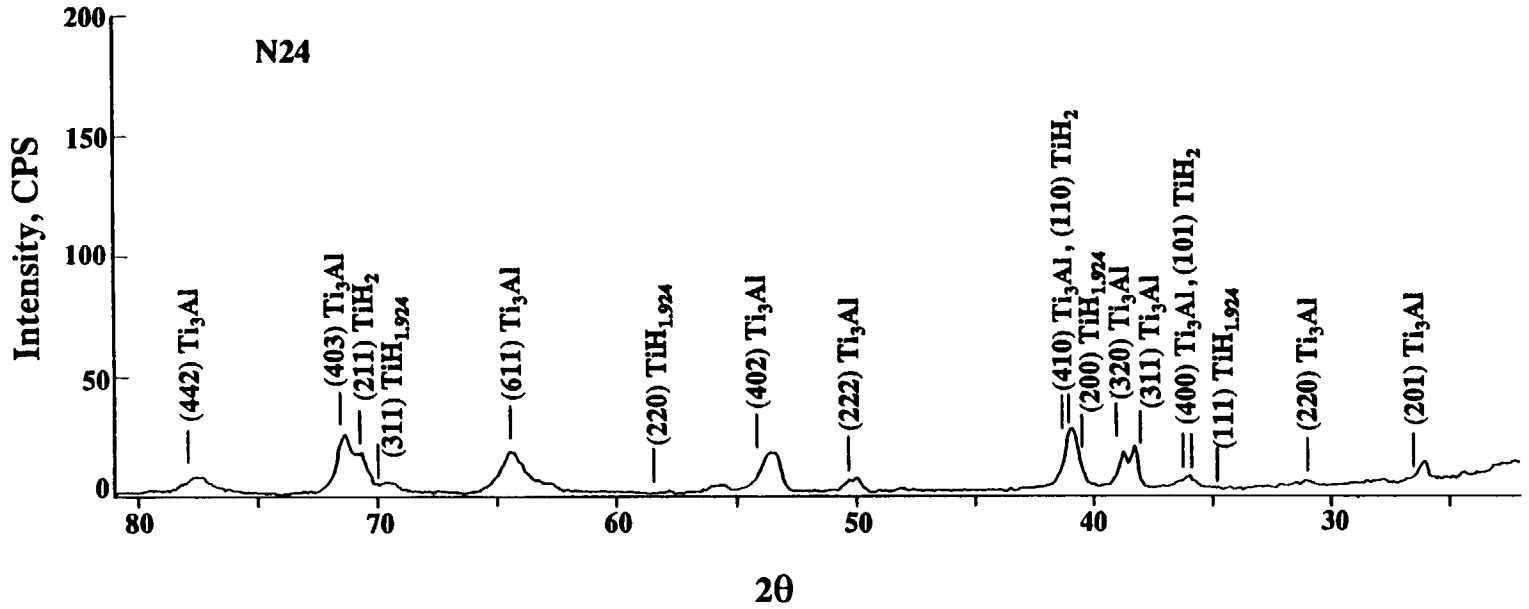


(d)

Figure 19. (cont'd) XRD patterns for Ti-24Al-11Nb: (d) $Ti_3Al$, $TiH_2$ and $TiH_{1.924}$ patterns observed in specimen N24 which was cracked after H-charging (3910 wt. ppm hydrogen).

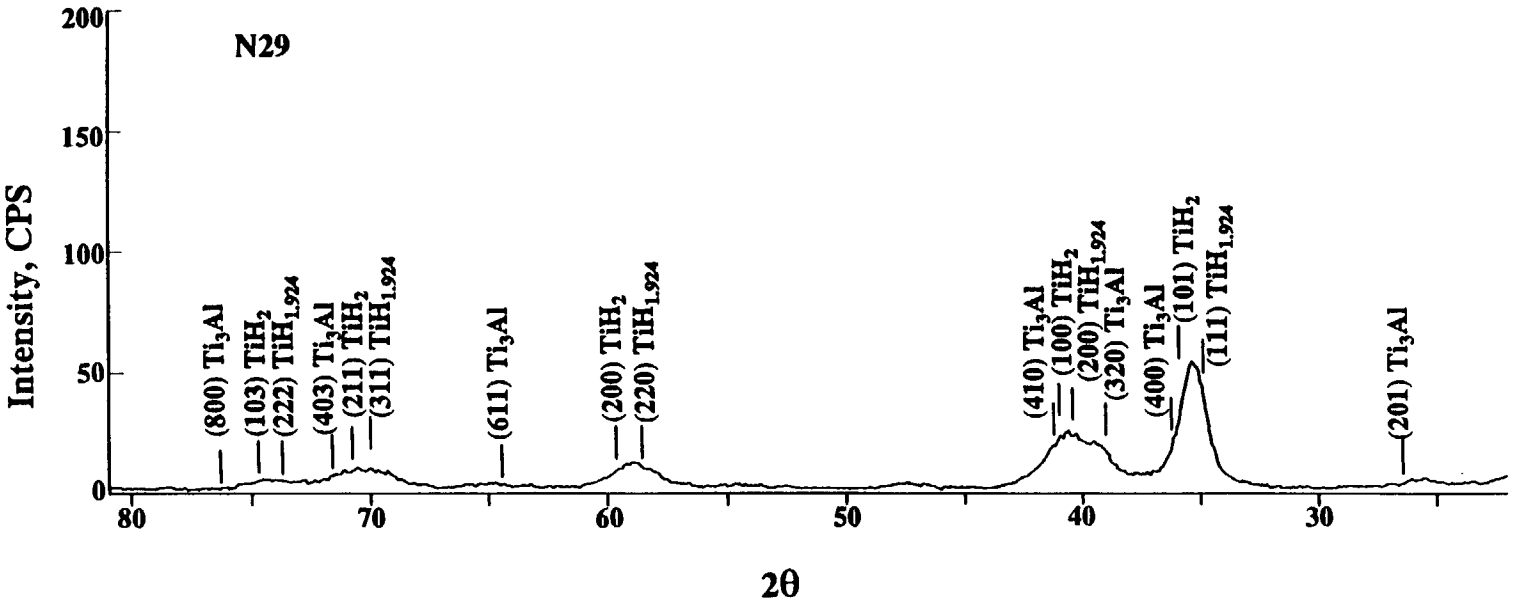


(e)

Figure 19. (cont'd) XRD patterns for Ti-24Al-11Nb: (e) $TiH_2$ plus $TiH_{1.924}$ patterns in specimen N29 which was pulverized after H-charging (19,400 wt. ppm hydrogen).

load crack growth behaviors of the fine basketweave material at either 25 or 600°C. At 25°C, a two percent plastic elongation was maintained at 1520 wt. ppm hydrogen, and the fracture toughness decreased from 15 MPa$\sqrt{m}$ at 39 wt. ppm hydrogen to 12.6 MPa$\sqrt{m}$ at 2750 wt. ppm hydrogen. On the other hand, the fine basketweave microstructure exhibited severe cracking and even pulverization during hydrogen charging under zero load when the hydrogen content exceeded approximately 3000 wt. ppm. This type of severe cracking and pulverization behavior has been observed previously in Ti-25Al-10Nb-3V-1Mo [16], and is not limited to Ti-24Al-11Nb only.

To understand the dichotomous behaviors, it is necessary to understand the mechanism that causes pulverization. Such an understanding can be provided by correlating the XRD results shown in Table V with the hydrogen content and specimen condition. Figure 20 shows that intact specimens were obtained for hydrogen contents less than 1500 wt. ppm, despite the formation of $TiH_2$-type hydrides. On the other hand, the occurrence of severe cracking during hydrogen charging coincided with the formation of $TiH_{1.924}$-type hydrides. Pulverization of the test specimens occurred when $Ti_3Al$ was completely converted into the $TiH_2$- and $TiH_{1.924}$-type hydrides. The result clearly demonstrates the detrimental effects of the $TiH_{1.924}$-type hydride on the integrity of the Ti-24-11 alloy. The crack pattern in Figure 17 suggests that cracking might be induced by large internal stresses, probably those associated with the formation of $TiH_{1.924}$-type hydrides.

The lack of influence of $TiH_2$-type hydrides on the tensile ductility of the Ti-24-11 alloy is in agreement with the previous study by Chan [15], who has observed that the fine basketweave microstructure is tolerant to hydrogen for up to 1300 wt. ppm hydrogen. The present results indicate that the limit of hydrogen tolerance of this microstructure is as high as 1500 wt. ppm for tensile ductility and 2750 wt. ppm for fracture toughness. The lack of a strong hydrogen effect on the stress rupture behavior is consistent with previous work by Jaffee and Williams [28], who showed that hydrogen did not reduce the stress rupture life of an $\alpha+\beta$ Ti-alloy with 800 wt. ppm hydrogen, despite the formation of hydrides in the microstructure. The lack of hydride embrittlement in the

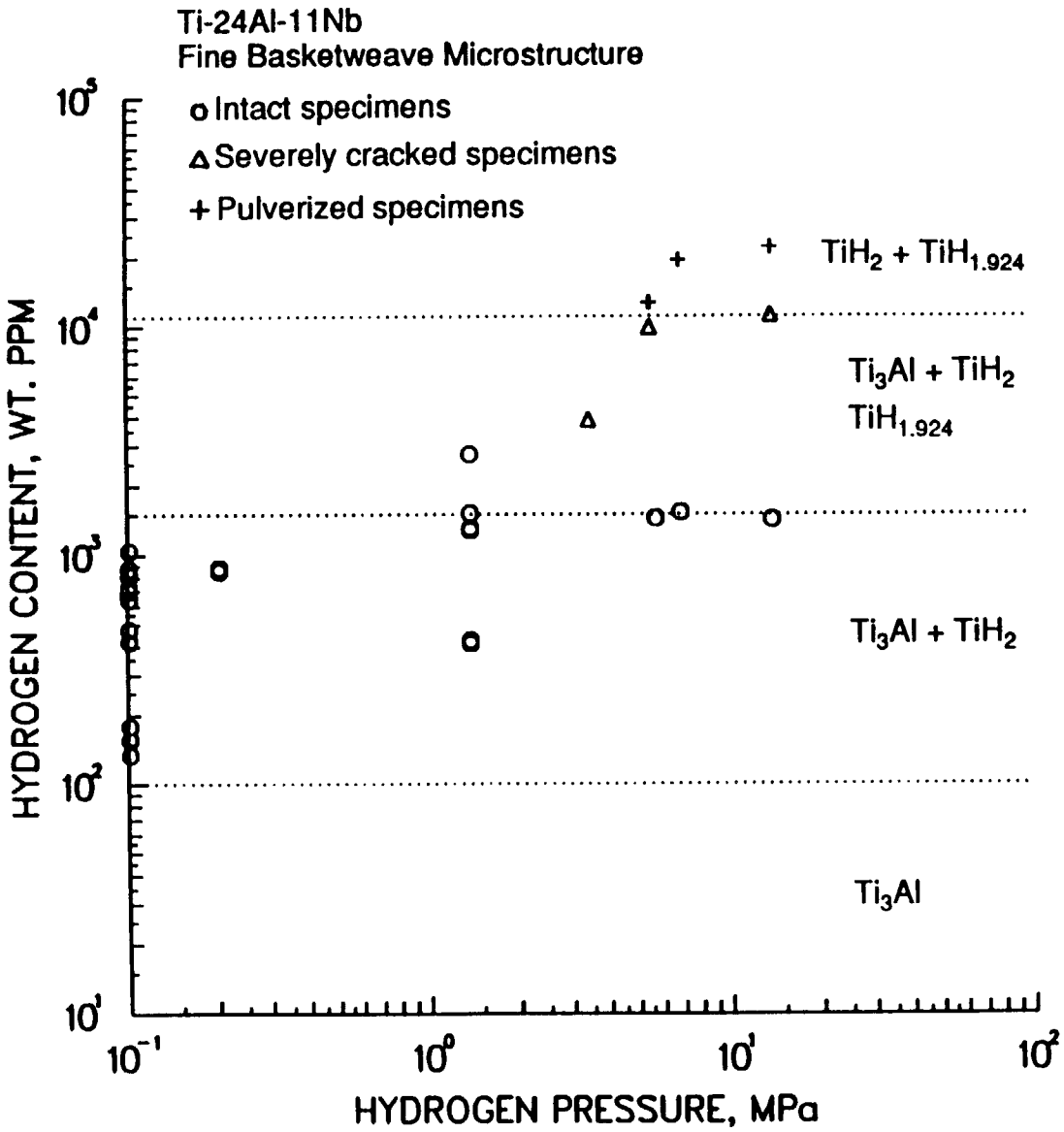


Figure 20. Correlations of hydrogen content, type of hydrides, and specimen conditions after H-charging for Ti-24Al-11Nb.

Ti-24-11 [15] and the α+β Ti-alloy [28] has been attributed to the discontinuous β phase in the microstructure, which prevents the formation of a continuous hydride network at the matrix/β interface and an easy path for crack propagation. This mechanism remains a plausible one for explaining the lack of hydride embrittlement in the Ti-24-11 alloy, provided that the hydride formed is the $TiH_2$-type and not the $TiH_{1.924}$ variety. Despite its ability to tolerate up to 1500 wt. ppm hydrogen, potential applications of the Ti-24-11 alloy with the fine basketweave microstructure as a structural material in a gaseous hydrogen environment appear unlikely because of the pulverization problem induced by $TiH_{1.924}$-type hydrides at hydrogen contents above 3000 wt. ppm. Previous work has shown that hydrogen embrittlement in Ti-24-11 is microstructure-sensitive [15]. Another key result provided by the present investigation is that besides microstructure, hydrogen embrittlement in the Ti-24-11 alloy depends on the hydrogen content and on the type of hydrides formed.

## CONCLUSIONS

1. Ti-24Al-11Nb with the fine basketweave microstructure is tolerant to hydrogen for hydrogen contents at least up to 1500 wt. ppm when the hydride formed in the microstructure is of the $TiH_2$-type.

2. Severe cracking and pulverization of the Ti-24Al-11Nb alloy occurs when the hydrogen content exceeds 3000 wt. ppm. Internal tensile stresses associated with the formation of $TiH_{1.924}$-type hydrides appears to be the cause of pulverization.

3. Hydrogen embrittlement in the Ti-24-11 alloy depends on microstructure, hydrogen content, and type of hyrides formed in the microstructure.

## ACKNOWLEDGEMENTS

The author is grateful for the support of this work by the NASA-AMES through TEES Subcontract No. 90-545 to Prime NAGS-283, and Dr. H. G. Nelson, Program Monitor. The technical assistance by Messrs. R. D. Brown, F. S. Campbell, H. G. Saldana, and J. F. Spencer, the clerical assistance by Ms. J. A. McCombs, and the editorial assistance by Ms. D. J. Stowitts, all of SwRI, are acknowledged. The author is also grateful for helpful discussions of this work by Drs. G. R. Leverant and R. A. Page of SwRI.

## REFERENCES

1. H. G. Nelson (ed.), **Proceedings of the Second Workshop on Hydrogen-Materials Interactions**, NASP Workshop Publication 1004, 1988.

2. H. G. Nelson (ed.), **Proceedings of the Third Workshop on Hydrogen-Materials Interactions**, NASP Workshop Publication 1007, 1990.

3. D. S. Shih, G. K. Scarr, and G. E. Wasielewski: **Proceedings of the Second Workshop on Hydrogen-Materials Interactions**, NASP Workshop Publication 1004, H. G. Nelson, ed., p. 136.

4. D. S. Shih, G. K. Scarr, and G. E. Wasielewski: *Scripta Met.*, 1989, vol. 23, pp. 973-978.

5. M. Gao, J. B. Boodey, and R. P. Wei: **Proceedings of the Third Workshop on Hydrogen-Materials Interactions**, NASP Workshop Publication 1007, H. G. Nelson, ed., 1990, pp. 117-124.

6. E. Manor and D. Eliezer: *Scripta Met.*, Vol. 23, 1989, pp. 1313-1318.

7. W. Y. Chu, A. W. Thompson, and J. C. Williams: **Hydrogen Effects on Material Behavior,** edited by N. Moody and A. W. Thompson, TMS, Warrendale, PA, 1990, pp.543-554.

8. S. Sullivan: **Proceedings of the Second Workshop on Hydrogen-Materials Interactions,** NASP Workshop Publication 1004, H. G. Nelson, ed., 1988, pp. 142-148.

9. K. Tosi and C. Smith: Presented at **NASP Fourth Workshop: Hydrogen-Material Interations,** Scottsdale, AZ, May 30 - June 1, 1990.

10. R. Jewett and D. Matejczyk: **Proceedings of the Second Workshop on Hydrogen-Materials Interactions,** NASP Workshop Publication 1004, H. G. Nelson, ed., 1988, pp. 137-139.

11. R. H. Barkalow: Presented at **NASP Third Workshop: Hydrogen-Materials Interaction,** Scottsdale, AZ, May 31-June 2, 1989.

12. L. G. Fritzemeier, M. A. Jacinto, and G. D. Schnittgrund: **Proceedings of the Third Workshop on Hydrogen-Materials Interactions,** NASP Workshop Publication 1007, H. G. Nelson, ed., 1990, pp. 117-124.

13. A. A. Sheinker and S. M. El-Soudani: **Proceedings of the Third Workshop on Hydrogen-Materials Interactions,** NASP Workshop Publication 1007, H. G. Nelson, ed., 1990, pp. 139-148.

14. S. M. Sastry, W. O. Soboyejo, and R. J. Lederich: **Proceedings of the Third Workshop on Hydrogen-Materials Interactions,** NASP Workshop Publication 1007, H. G. Nelson, ed., 1990, pp. 191-200.

15. K. S. Chan: *Met. Trans. A*, vol. 23A, 1992, pp. 497-507.

16. B. S. Majumdar, H. J. Cialone, and J. H. Holbrook: **Proceedings of the Third Workshop on Hydrogen-Materials Interactions**, NASP Workshop Publication 1007, H. G. Nelson, ed., 1990, pp. 73-87, Scottsdale, AZ, June 1-3, 1988.

17. K. S. Chan: *Met. Trans. A*, vol. 23A, 1992, pp. 183-200.

18. A. Nagy, J. B. Campbell, and D. L. Davidson: *Rev. Sci. Instrum.*, 1984, vol. 55, pp. 778-782.

19. JCPDS Powder Diffraction File, Joint Committee on Powder Diffraction Standards, Swarthmore, PA, 1974.

20. P. S. Rudman, J. J. Reilly, and R. H. Wiswall: *J. Less-Common Mater.*, Vol. 58, 1978, pp. 231-240.

21. D. E. Matejczyk and C. G. Rhodes: *Scripta Metall.*, Vol. 24, 1990, pp. 1369-1373.

22. D. Legzdina, I. M. Robertson, and H. K. Birnbaum: *J. Mater. Res.*, Vol. 6, 1991, pp. 1230-1237.

23. O. T. Woo, G. C. Weatherby, C. E. Coleman, and R. W. Gilbert: *Acta Metall.*, Vol. 33, 1985, pp. 1897-1906.

24. H. Numakura and M. Koiwa: *Acta Metall.*, Vol 32, 1984, pp. 1799-1807.

25. D. S. Shih and H. K. Birnbaum: *Scripta Metall.*, Vol. 20, 1986, pp. 1261-1264.

26. H. L. Yaket, Jr.: *Acta Crystall.*, Vol. 11, 1958, pp. 46-51.

27. S. S. Sidhu, L. Heaton, and D. D. Zauberis: *Acta Crystall.*, Vol. 9, 1956, pp. 607-614.

28. R. I. Jaffee and D. N. Williams: *Transactions of ASM*, Vol. 51, 1959, pp. 820-842.

## Table I
## Summary of Hydrogen Charging Conditions and Results for Coupon, Tensile, Creep, and Fracture Specimens

| Test No. | Specimen No. | Hydrogen Pressure, Psi | Charging Temperature, °C | Time of $H_2$ Charging, Hrs | Heating Rate, °C/hr | Specimen Condition After $H_2$ Charging | Hydrogen Content,* wt. ppm. | $H_2$ Charging Apparatus |
|---|---|---|---|---|---|---|---|---|
| 1 | N3 | 3000 | 550 | 100 | 32°C/hr | pulverized | --- | large autoclave |
| 2 | N4 | 3000 | 550 | 24 | 38°C/hr | pulverized | --- | large autoclave |
| 3 | N5 | 2000 | 538 | 24 | 25°C/hr | pulverized | --- | large autoclave |
| 4 | N6 (electropolished) | 2000 | 538 | 24 | 35°C/hr | pulverized | > 5000* | large autoclave |
| | N7 (600 μm finish) | 2000 | 538 | 24 | 35°C/hr | pulverized | --- | large autoclave |
| | O1 (electropolished) | 2000 | 538 | 24 | 35°C/hr | cracked, but not pulverized | > 5000* | large autoclave |
| | O2 (600 μm finish) | 2000 | 538 | 24 | 35°C/hr | cracked, but not pulverized | 11,180 | large autoclave |
| 5 | N1 | 97 | 430 ± 25 | 54 | 28°C/hr | intact | 98* | large autoclave |
| 6 | N2 | 50 | 430 ± 25 | 120 | 25°C/hr | intact | 32* | large autoclave |

**Table I**
**Summary of Hydrogen Charging Conditions and Results for Coupon, Tensile, Creep, and Fracture Specimens (cont'd)**

| Test No. | Specimen No. | Hydrogen Pressure, Psi | Charging Temperature, °C | Time of $H_2$ Charging, Hrs | Heating Rate, °C/hr | Specimen Condition After $H_2$ Charging | Hydrogen Content,* wt. ppm. | $H_2$ Charging Apparatus |
|---|---|---|---|---|---|---|---|---|
| 7 | N8 | 1000 | 538 | 100 | 402°C/hr | intact | 630*, 690* | hydrogen stress rupture test (creep) apparatus |
| | O4 | 1000 | 538 | 100 | 402°C/hr | intact | --- | hydrogen stress rupture test (creep) apparatus |
| | 29 (tensile) | 1000 | 538 | 100 | 402°C/hr | intact | 1520 | hydrogen stress rupture test (creep) apparatus |
| 8 | N9 | 2000 | 538 | 100 | 181°C/hr | intact | 270*, 270* | hydrogen stress rupture test (creep) apparatus |
| | O3 | 2000 | 538 | 100 | 181°C/hr | intact | 550* | hydrogen stress rupture test (creep) apparatus |
| | 30 (tensile) | 2000 | 538 | 100 | 181°C/hr | intact | --- | hydrogen stress rupture test (creep) apparatus |

**Table I**
**Summary of Hydrogen Charging Conditions and Results for Coupon, Tensile, Creep, and Fracture Specimens (cont'd)**

| Test No. | Specimen No. | Hydrogen Pressure, Psi | Charging Temperature, °C | Time of $H_2$ Charging, Hrs | Heating Rate, °C/hr | Specimen Condition After $H_2$ Charging | Hydrogen Content,* wt. ppm. | $H_2$ Charging Apparatus |
|---|---|---|---|---|---|---|---|---|
| 9 | N10 | 2500 | 538 | 50 | 180°C/hr | pulverized | --- | small autoclave |
| | O5 | 2500 | 538 | 50 | 180°C/hr | pulverized | --- | small autoclave |
| | E1 | 2500 | 538 | 50 | 180°C/hr | pulverized | --- | small autoclave |
| 10 | O6 | 2500 | 538 | 10 | 510°C/hr | pulverized | --- | small autoclave |
| 11 | N11 | 2500 | 538 | 2 | 510°C/hr | pulverized | --- | small autoclave |
| | O7 | 2500 | 538 | 2 | 510°C/hr | pulverized | --- | small autoclave |
| 12 | N12 | 2000 | 538 | 100 | 510°C/hr | pulverized | --- | small autoclave |
| | O8 | 2000 | 538 | 100 | 510°C/hr | pulverized | --- | small autoclave |
| 13 | N13 | 2000 | 538 | 2 | 165°C/hr | pulverized | --- | small autoclave |
| 14 | N14 | 2000 | 482 | 2 | 193°C/hr | intact, pitted | 130* | small autoclave |

**Table I**
**Summary of Hydrogen Charging Conditions and Results for Coupon, Tensile, Creep, and Fracture Specimens (cont'd)**

| Test No. | Specimen No. | Hydrogen Pressure, Psi | Charging Temperature, °C | Time of $H_2$ Charging, Hrs | Heating Rate, °C/hr | Specimen Condition After $H_2$ Charging | Hydrogen Content,* wt. ppm. | $H_2$ Charging Apparatus |
|---|---|---|---|---|---|---|---|---|
| 15 | N16<br>N22 | 2000 | 482 | 2 | 193°C/hr | intact, cracked | --- | small autoclave |
| 16 | N17 | 2000 | 482 | 3 | 193°C/hr | pulverized | 22,000 | small autoclave |
| 17 | N19 | 2000 | 482 | 1 | 193°C/hr | intact | --- | small autoclave |
| 18 | N25 | 2000 | 482 | $1\frac{1}{2}$ | 193°C/hr | intact | 69* | small autoclave |
| 19 | N26 | 2000 | 482 | $2\frac{1}{2}$ | 193°C/hr | intact | --- | small autoclave |
| 20 | N20 | 1350°F/$\frac{1}{2}$ hr/1 atm. He; followed by 1000°F/16 hrs/1 atm. He + 1 atm. $H_2$ | | | 193°C/hr | intact | 2400*, 2600* | small autoclave |
| 21 | N21 | 1350°F/$\frac{1}{2}$ hr/2 atm. $H_2$; followed by 1000°F/50 hrs/2 atm. $H_2$ | | | 193°C/hr | intact | 850*, 880* | small autoclave |
| 22 | N27 | 1350°F/1 hr/1 atm. He; followed by 1000°F/40 hrs/1 atm. $H_2$ + 1 atm. He | | | 193°C/hr | intact | 2000* | small autoclave |

**Table I**
**Summary of Hydrogen Charging Conditions and Results for Coupon, Tensile, Creep, and Fracture Specimens**
**(cont'd)**

| Test No. | Specimen No. | Hydrogen Pressure, Psi | Charging Temperature, °C | Time of $H_2$ Charging, Hrs | Heating Rate, °C/hr | Specimen Condition After $H_2$ Charging | Hydrogen Content,* wt. ppm. | $H_2$ Charging Apparatus |
|---|---|---|---|---|---|---|---|---|
| 23 | N23 | 1350°F/$\frac{1}{2}$ hr/1 atm. He; followed by 16 hrs/1 atm. He + 200 psi. $H_2$ at 1000°F | | | 193°C/hr | intact | 2200*, 990* 1422 | small autoclave |
| 24 | N24 | 1350°F/1 hr/1 atm. He; followed by 16 hrs/1 atm. + 500 psi. $H_2$ at 1000°F | | | 193°C/hr | intact, surface cracks | 2600*, 1000* 3910 | small autoclave |
| 25 | N28 | 1350°F/$\frac{1}{2}$ hr/1 atm. He; followed by 16 hrs/1 atm. He + 830 psi. $H_2$ at 1000°F | | | 193°C/hr | intact | 2000* 1440 | small autoclave |
| 26 | N29 | 1350°F/$\frac{1}{2}$hr/1 atm. He; followed by 16 hrs/1 atm. He + 830 psi. $H_2$ at 1000°F | | | 193°C/hr | pulverized | 19,400 | small autoclave |
| 27 | N30 | 1350°F/$\frac{1}{2}$hr/1 atm. He; followed by 16 hrs/1 atm. He + 830 psi. $H_2$ at 1000°F | | | 193°C/hr | pulverized | 12,670 | small autoclave |
| | 36 | 1350°F/$\frac{1}{2}$hr/1 atm. He; followed by 16 hrs/1 atm. He + 830 psi. $H_2$ at 1000°F | | | 193°C/hr | severely cracked | 9880 | small autoclave |

**Table I**
**Summary of Hydrogen Charging Conditions and Results for Coupon, Tensile, Creep, and Fracture Specimens (cont'd)**

| Test No. | Specimen No. | Hydrogen Pressure, Psi | Charging Temperature, °C | Time of $H_2$ Charging, Hrs | Heating Rate, °C/hr | Specimen Condition After $H_2$ Charging | Hydrogen Content,* wt. ppm. | $H_2$ Charging Apparatus |
|---|---|---|---|---|---|---|---|---|
| 28 | 325 (CT) | 1350°F/½hr/1 atm. He; followed by 16 hrs/1 atm. $H_2$ + 1 atm. $H_2$ at 1000°F | | | 193°C/hr | intact | 156 | small autoclave |
| | 31 (Tensile) | 1350°F/½hr/1 atm. He; followed by 16 hrs/1 atm. $H_2$ + 1 atm. $H_2$ at 1000°F | | | 193°C/hr | intact | 179, 360* | small autoclave |
| | 32 (Tensile) | 1350°F/½hr/1 atm. He; followed by 16 hrs/1 atm. $H_2$ + 1 atm. $H_2$ at 1000°F | | | 193°C/hr | intact | 640 | small autoclave |
| 29 | N32 | 1350°F/½hr/1 atm. He; followed by 16 hrs/1 atm. $H_2$ + 1 atm. He at 100°F | | | 193°C/hr | intact | 474 | small autoclave |
| | 326 (CT) | 1350°F/½hr/1 atm. He; followed by 16 hrs/1 atm. $H_2$ + 1 atm. He at 100°F | | | 193°C/hr | intact | 419 | small autocalve |
| | 37 (Tensile) | 1350°F/½hr/1 atm. He; followed by 16 hrs/1 atm. $H_2$ + 1 atm. He at 100°F | | | 193°C/hr | intact | 816 | small autoclave |
| | 38 (Tensile) | 1350°F/½hr/1 atm. He; followed by 16 hrs/1 atm. $H_2$ + 1 atm. He at 100°F | | | 193°C/hr | intact | 1045 | small autoclave |

**Table I**
**Summary of Hydrogen Charging Conditions and Results for Coupon, Tensile, Creep, and Fracture Specimens (cont'd)**

| Test No. | Specimen No. | Hydrogen Pressure, Psi | Charging Temperature, °C | Time of $H_2$ Charging, Hrs | Heating Rate, °C/hr | Specimen Condition After $H_2$ Charging | Hydrogen Content,* wt. ppm. | $H_2$ Charging Apparatus |
|---|---|---|---|---|---|---|---|---|
| 29 | 39 (Tensile) | 1350°F/½hr/1 atm. He; followed by 16 hrs/1 atm. $H_2$ + 1 atm. He at 100°F | | | 193°C/hr | intact | 875 | small autoclave |
| | 40 (Tensile) | 1350°F/½hr/1 atm. He; followed by 16 hrs/1 atm. $H_2$ + 1 atm. He at 100°F | | | 193°C/hr | intact | --- | small autoclave |
| 30 | N33 | 1350°F/½hr/1 atm. He; followed by 16 hrs/1 atm. $H_2$ + 1 atm. He at 100°F | | | 193°C/hr | intact | 596 | small autoclave |
| | 327 (CT) | 1350°F/½hr/1 atm. He; followed by 16 hrs/1 atm. $H_2$ + 1 atm. He at 100°F | | | 193°C/hr | intact | 134 | small autoclave |
| | 44 (Tensile) | 1350°F/½hr/1 atm. He; followed by 16 hrs/1 atm. $H_2$ + 1 atm. He at 100°F | | | 193°C/hr | intact | 720 | small autoclave |
| 31 | N31 | 1350°F/½hr/1 atm. He; followed by 16 hrs/1 atm. He + 200 psi $H_2$ at 1000°F | | | 193°C/hr | intact | 410 | small autoclave |
| | 45 (tensile) | 1350°F/½hr/1 atm. He; followed by 16 hrs/1 atm. He + 200 psi $H_2$ at 1000°F | | | 193°C/hr | intact | 1518 | small autoclave |

**Table I**
**Summary of Hydrogen Charging Conditions and Results for Coupon, Tensile, Creep, and Fracture Specimens**
**(cont'd)**

| Test No. | Specimen No. | Hydrogen Pressure, Psi | Charging Temperature, °C | Time of $H_2$ Charging, Hrs | Heating Rate, °C/hr | Specimen Condition After $H_2$ Charging | Hydrogen Content,* wt. ppm. | $H_2$ Charging Apparatus |
|---|---|---|---|---|---|---|---|---|
| 31 | 46 (tensile) | 1350°F/½hr/1 atm. He; followed by 16 hrs/1 atm. He + 200 psi $H_2$ at 1000°F | | | 193°C/hr | intact | 1277 | small autoclave |
| | 47 (tensile) | 1350°F/½hr/1 atm. He; followed by 16 hrs/1 atm. He + 200 psi $H_2$ at 1000°F | | | 193°C/hr | intact | 1307 | small autoclave |
| 32 | N34 | 1350°F/½hr/1 atm. He; followed by 16 hrs/1 atm. He + 200 psi $H_2$ at 1000°F | | | 193°C/hr | intact | 425 | small autoclave |
| | 317 (SEN) | 1350°F/½hr/1 atm. He; followed by 16 hrs/1 atm. He + 200 psi $H_2$ at 1000°F | | | 193°C/hr | intact | 2750 | small autoclave |

* Hydrogen contents were determined by either Luvak in Boylston, MA or by National Spectrographic Laboratories (NSL) in Cleveland, OH. All unasterisked results were obtained by Luvak, while the NSL results are asterisked.

## Table II

## Test Matrix for Evaluating the Limit of Hydrogen Tolerance of the Ti-24Al-11Nb Alloy with the Fine Basketweave Microstructure

| Task 1: Tensile Tests of $H_2$-Charged Specimens | | | | | | | | |
|---|---|---|---|---|---|---|---|---|
| | Hydrogen Content, wt. ppm | | | | | | | |
| T, C° | 60 (As heat-treated) | 160 | 220 | 640 | 720 | 880 | 1300 | 1500 |
| 25 | X O43 | X | X O31 | | O44 | O39 | X | O29 |
| 600 | X | | | O32 | | | | O45 |
| Task 2: Fracture Toughness of H-Charged Specimens | | | | | | | | |
| | Hydrogen Content, wt. ppm | | | | | | | |
| T, C° | 60 (As heat-treated) | | 150 | | 420 | | 2750 | |
| 25 | X | | O325 | | | | O317 | |
| 600 | X | | | | O326 | | | |
| Task 3: Constant-Load Creep Tests of $H_2$ Charged Specimens | | | | | | | | |
| | Hydrogen Content, wt. ppm | | | | | | | |
| T, C° | 60-80 (As heat-treated) | | 640 | | 1000 | | 1300 | |
| 25 | O41 | | O37 | | | | X O45 | |
| 600 | O42 | | | | O38 | | O47 | |
| Task 4: Sustained-Load Crack Growth Tests | | | | | | | | |
| | Hydrogen Content, wt. ppm | | | | | | | |
| T, C° | 60 (As heat-treated) | | | 134 | | | | |
| 600 | O328 | | | O327 | | | | |

X - Data available from other SwRI programs.
O - Completed tests and specimen identification for this program.

## Table III

**Summary of Tensile Results of H-Charged and Uncharged Ti-24Al-11Nb with the Fine Basketweave Microstructure. The Nominal Strain Rate was $5 \times 10^{-6}$ $sec^{-1}$.**

| Specimen | T, °C | $H_2$-Exposure | $H_2$ Content (wt. ppm) | Yield Stress (MPa) | Ultimate Tensile Strength (MPa) | Total Elongation (%) | Plastic Elongation (%) |
|---|---|---|---|---|---|---|---|
| 9 [15] | 25 | unexposed | 67 | 688.4 | 842.6 | 3.08 | 1.88 |
| 43 | 25 | unexposed | 70 | 550.0 | 826.7 | 8.50 | 7.24 |
| 7 [15] | 25 | exposed[a] | 220 | 704.5 | 746.6 | 2.63 | 1.27 |
| 8 [15] | 25 | exposed[a] | 160 | 730.5 | 853.6 | 5.30 | 4.02 |
| 23 [15] | 25 | exposed[b] | 1300 | 535.7 | 659.0 | 2.75 | 1.90 |
| 24 [15] | 25 | exposed[b] | 1300 | 530.2 | 690.9 | 3.25 | 2.10 |
| 29 | 25 | exposed[b] | 1530 | 612.1 | 745.5 | 2.70 | 1.55 |
| 31 | 25 | exposed[c] | 270 | 545.5 | 700.0 | 3.10 | 2.10 |
| 44 | 25 | exposed[c] | 720 | 564.7 | 641.1 | 1.86 | 1.0 |
| 32 | 600 | exposed[c] | 640 | 277.4 | 420.0 | 9.00 | 8.25 |
| 45 | 600 | exposed[c] | 1520 | 300.0 | 424.2 | 8.70 | 8.20 |

Key: a -- prior creep at 316° for 100 hours under a constant initial stress of 586 MPa and 13.8 MPa hydrogen pressure.

b -- 100 hours in 6.9 to 13.8 MPa gaseous hydrogen at 538°C.

c -- 16 hours in 0.1 to 1.4 MPa gaseous hydrogen at 538°C.

## Table IV

**Summary of AES Results Obtained for H-Charged Ti-24Al-11Nb Coupon Specimens Compared to an Uncharged, Fresh Surface**

| Specimen | T, °C | $\dot{T}$, °C/hr | P, MPa | Time, hr | Thickness of Oxygen-Rich Layer, Å | Specimen* Condition After H-Charge |
|---|---|---|---|---|---|---|
| N2 | --- | --- | --- | --- | ≈ 400 Å | uncharged, fresh surface |
| N2 | 430 | 25 | 0.34 | 120 | 2400 Å | intact |
| 03 | 538 | 181 | 13.60 | 100 | 2000 Å | intact |
| N9 | 538 | 181 | 13.60 | 100 | 2000 Å | intact |
| N14 | 482 | 193 | 13.60 | 2 | ≈ 800 Å | pitted, but intact |
| 02 | 538 | 35 | 13.60 | 24 | less than 200 Å | pulverized |
| 06 | 538 | 35 | 17.00 | 10 | less than 400 Å | pulverized |

## Table V

### Summary of XRD Results for Hydrogen Charged and Undercharged Specimens of Ti-24Al-11Nb

| Specimen | Specimen Type | Condition after Hydrogen Charging | Hydrogen Content wt. ppm. | Phases Identified by XRD |
|---|---|---|---|---|
| 328 | fracture specimen | as heat treated | 70 | $Ti_3Al$ |
| 325 | fracture specimen | intact | 156 | $Ti_3Al + TiH_2$ |
| 326 | fracture specimen | intact | 419 | $Ti_3Al + TiH_2$ |
| 327 | fracture specimen | intact | 134 | $Ti_3Al + TiH_2$ |
| 31 | tensile specimen | intact | 179 | $Ti_3Al + TiH_2$ |
| N23 | coupon | intact | 1422 | $Ti_3Al + TiH_2 + TiH_{1.924}$ |
| 29 | tensile specimen | intact | 1520 | $Ti_3Al + TiH_2 + TiH_{1.924}$ |
| 317 | fracture specimen | intact + microcracks | 2750 | $Ti_3Al + TiH_2 + TiH_{1.924}$ |
| N24 | coupon | cracked | 3910 | $Ti_3Al + TiH_2 + TiH_{1.924}$ |

## Table V

**Summary of XRD Results for Hydrogen Charged and Undercharged Specimens of Ti-24Al-11Nb (continued)**

| Specimen | Specimen Type | Condition after Hydrogen Charging | Hydrogen Content wt. ppm. | Phases Identified by XRD |
|---|---|---|---|---|
| 02 | coupon | severely cracked | 11,180 | $Ti_3Al + TiH_2 + TiH_{1.924}$ |
| N4 | coupon | pulverized | --- | $TiH_2 + TiH_{1.924}$ |
| N17 | coupon | pulverized | 22,000 | $TiH_2 + TiH_{1.924}$ |
| N29 | coupon | pulverized | 19,400 | $TiH_2 + TiH_{1.924}$ |